VIETNAM NATIONAL UNIVERSITY, HANOI

HANOI UNIVERSITY OF SCIENCES

FACULTY OF PHYSICS

KIM THI PHUONG

THE BLACK HOLE IN THE CENTRE OF THE MILKY WAY

DIPLOMA IN THEORETICAL PHYSICS

HANOI, MAY - 2006

VIETNAM NATIONAL UNIVERSITY, HANOI
HANOI UNIVERSITY OF SCIENCES
FACULTY OF PHYSICS

KIM THI PHUONG

THE BLACK HOLE IN THE CENTRE OF THE MILKY WAY

DIPLOMA IN THEORETICAL PHYSICS

Supervisors: DR. PHAM THUC TUYEN AND
PROF. PIERRE DARRIULAT

HANOI, MAY - 2006

ACKNOWLEDGEMENTS

I would like to thank all teachers in the Faculty of Physics and the Department of Theoretical Physics who trained me throughout last years.

This work was performed in the Vietnam Auger Training LaboratorY (VATLY). I thank Dr. VO VAN THUAN for having welcoming me in his Institute, and the research team of VATLY for the help and support that they patiently gave me throughout my work.

I am very grateful to my parents for bringing me up and making me best conditions to study so far. I am thankful to my other relatives and my friends for their encouragement and help.

Finally, I would like to express my heartfelt and deep gratitude to those who guided me through this study, Dr. PHAM THUC TUYEN and Prof. PIERRE DARIULAT.

Hanoi 15-05-2006

Kim Thi Phuong

CONTENTS

CHAPTER 1

BLACK HOLES: AN OVERVIEW

Black holes are very massive celestial objects that play an important role in the universe. One of them, Sagittarius A* (Sgr A*), having a mass of over 3 million solar masses, is located at the centre of the Milky Way, our galaxy. It is the subject of the present study.

A black hole is the seat of such a strong gravitational field that nothing, not even light, can escape from the interior of its horizon, a sphere having a radius (the Schwarzschild radius) proportional to its mass. When an object approaches a black hole from outside its horizon, it is subjected to a strong gravitational pull and to important tidal forces that tear it apart. While some of its material disappears beyond the horizon of the black hole, an important flux of radiation is emitted outwards, making the black hole appear as a bright object.

We know today of several black holes in the universe. Some are the final product of the gravitational collapse that takes place at the end of the life of massive stars (supernovae). They are called stellar black holes and have masses of a few solar masses[1] (star masses never exceed 100 or so solar masses and only their cores contract into a black hole, their envelopes are ejected outwards). We expect the Milky Way to contain some 10^8 such black holes (out of 10^{11} stars). Others are much more massive and are located at the centres of galaxies; they are called galactic black holes. Their masses may reach very large values, up to many billion solar masses. We have reasons today to expect that each galaxy has a galactic black hole in its centre and that it is the result of the merging of many stellar black holes.

In the present section we shall give a very simple presentation of the properties of black holes, starting with elementary kinematical and dynamical

[1] Indeed star masses (M) in galaxies such as ours never exceed 100 or so solar masses (the heaviest such stars are called Wolf-Rayet stars and have masses that may reach 120 solar masses). The lighter main sequence stars burn their hydrogen using the pp cycle and their lifetime is long, inversely proportional to M^4 while the heavier main sequence stars use the more efficient CNO cycle and their lifetime is short, inversely proportional to M^2. In general the details of the nuclear reactions taking place inside the star define its stability, its maximum possible mass and its lifetime in a very sensitive way.

considerations, continuing with some comments on collisions and the mechanism of accretion and ending with an overview of black holes in the universe.

1.1. Elementary kinematical and dynamical considerations

First, we consider a homogeneous sphere having radius R_0, density ρ, and mass M. A mass $\mu << M$ at its surface is given an outward radial velocity V_0. We call $V(r)$ its velocity (at any distance $r > R_0$ on its trajectory). Energy conservation gives:

$$-\frac{K\mu}{2} = \frac{1}{2}\mu V_0^2 - G\mu\frac{M}{R_0} = \frac{1}{2}\mu V^2(r) - G\mu\frac{M}{r} \tag{1}$$

The fact that a same mass μ enters both the expression of the kinetic energy (inertial mass) and that of the gravitational potential (gravitational mass) is an essential feature of gravity. It leads to the principle of equivalence and to general relativity and implies that all masses have the same movement in a given gravitational field.

From (1) we get: $V^2(r) = 2G\frac{M}{r} - K$

When V_0 obeys the relation $K = 2G\frac{M}{R_0} - V^2(r) = 0$, V_0 is called the escape velocity:

$$V_{esc} = \sqrt{\frac{2GM}{R_0}} \tag{2}$$

For $V_0 > V_{esc}$, namely $K = V_{esc}^2 - V_0^2 < 0$, Eq.1 has always a solution. In particular, for $r = \infty, V(\infty) = \sqrt{-K}$ and the mass μ escapes the attraction of the gravitational field.

For $V_0 < V_{esc}$, namely $K = V_{esc}^2 - V_0^2 > 0$, Eq.(1) has no solution for $r > 2G\frac{M}{K}$ corresponding to $V(r) = 0$. After having reached this extreme point, the mass μ falls back toward the field source and does not escape the attraction of its gravitational field.

In order to illustrate these features we have integrated Eq.(1) in the case of the Earth ($R_0 = 6380km$ and $\frac{GM}{R_0^2} = g = 9.81\, m/s^2$, $V_{esc} = 11.2km/s$) for various values of V_0. The results are shown on Figure 1. 1

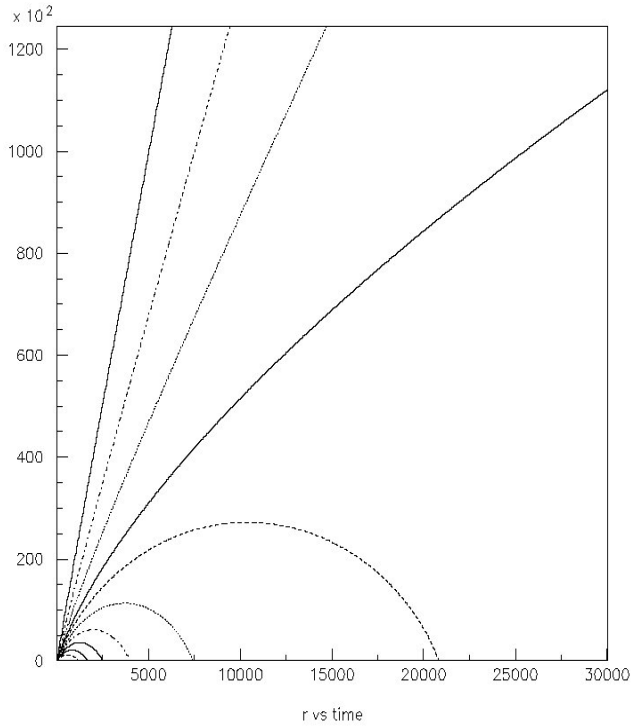

Figure 1.1 The dependence of altitude on time for a projectile launched vertically from the earth with velocities V_0 equal to 0.4, 0.5, 0.6, 0.7, 0.8, 0.9, 1, 1.2, 1.5 and 2 V_{esc} respectively where the escape velocity V_{esc} is 11.2km/s.
The ordinate shows the altitude in kilometers (it reaches 27200km in the case V_0/V_{esc}=0.9). The abscissa is the time in seconds.

From the expression of the escape velocity we see that when an object of mass M has a radius

$$R_{Sch} = 2G\frac{M}{c^2} \tag{3}$$

called its Schwarzschild radius, the escape velocity on its surface reaches the velocity of light: the above non-relativistic calculation is no longer valid and a relativistic calculation must be done instead. However its result happens to be the same: when a spherical object has a radius equal to (or smaller than) its Schwarzschild radius (as defined above) no energy can escape from it in any form,

whether matter or radiation. Indeed we know that in the relativistic case it is energy that weighs, not matter, and the principle of equivalence tells us that photons are bent in the gravitational field as are massive particles. One calls such an object a black hole.

The sphere having the Schwarzschild radius as its radius is called the horizon of the black hole. Any object that is smaller than its horizon is therefore a black hole. The expression "black hole" was coined by J.A. Wheeler, "black" meaning that no light can escape from it and "hole" implying that anything that falls beyond its horizon is lost forever.

The Schwarzschild radii of a few objects are listed in the table below:

Object	Radius	Mass (solar masses)	R_{Sch}
Earth	6 380 km	$3\ 10^{-6}$	9 mm
Sun	$7\ 10^{5}$ km	1	3 km
Sgr A*	Black hole	$3\ 10^{6}$	10^{7} km
Cygnus X-1	Stellar black hole	10	30 km
Cygnus A	Galactic black hole	$5\ 10^{9}$	$1.5\ 10^{10}$ km
Nuclear matter	9 km	3	9 km

For a sphere of uniform density having a mass of 3 solar masses $\approx 3 \cdot 10^{57} GeV$ and having its radius equal to its Schwarzschild radius, $R \approx 9km$, the density is $\approx \frac{3 \cdot 10^{57}}{729 \cdot \frac{4}{3}\pi} GeV/km^3 \approx 1 GeV/fm^3$. These numbers are close to the parameters of a typical neutron star (about twice the Chandrasekhar limit) and of the density of nuclear matter.

When a neutron star having a radius just above its Schwarzschild radius acquires some mass (because of matter from its environment falling on it) its radius increases less rapidly than its mass (as the cubic root of the mass if the star were homogeneous; but it is not, it is structured in concentric layers) but its

Schwarzschild radius increases in proportion to the mass: at some point its Schwarzschild radius exceeds its radius and the star becomes a black hole. Seen from outside, not much happens then: the gravitational field increases slowly through the transition as if nothing special had happened. Once the star has become a black hole, nothing can escape from it; but there were already very few objects that could escape from it before it became a black hole and light was already very strongly red shifted: again, nothing dramatic seems to be happening. In a frame attached to the surface of the star, crossing the horizon corresponds to no discontinuity. However, while the neutron star could resist gravity the black hole cannot any longer and will continue to shrink: general relativity tells us that the space is so strongly curved inside the horizon that no pressure can resist the gravitational pull. It is remarkable that such a dramatic event has nearly no detectable effect outside the horizon. The shrinkage would continue indefinitely if we believe general relativity but we know that something must happen at the scale of $\sim 10^{-33}$cm (corresponding to the Planck mass) where quantum mechanics and general relativity are no longer compatible. However, down to that scale, any new physics that may occur (for example we know of the quark-gluon deconfined phase but other effects may happen at higher densities) should be unable to stop the gravitational collapse of the star.

It is not quite true however that nothing can be seen from outside. It is only true in the case of a spherical static star free of magnetic field. Any deviation from perfect sphericity and any trapped magnetic field must disappear in the collapse: the final black hole should have “no hair” as one says; in particular it should be spherical and trap no magnetic field. In the process any trapped magnetic field is therefore converted into electromagnetic radiation (just outside the horizon) and the absorption of small irregularities produces gravitational waves. Both electromagnetic and gravitational waves are in principle detectable from outside the horizon.

In practice, however, black holes look usually quite different from what these comments tend to describe: they are embedded in an environment that has a very strong influence on their appearance.

1.2 Collisions and the mechanism of accretion.

From what we described in the preceding section, black holes should be invisible. However, in most cases, their environment contains matter that is attracted by them and forms a so-called accretion disk (Figure 1.2) around them before being swallowed beyond the horizon. This disk is the seat of collisions that cause its temperature to reach high values and therefore the emission of radiation. In many cases, as a result, we can see the accretion disk of the black hole that can be very bright. Moreover, when important amounts of matter fall beyond the black hole horizon it becomes the seat of very violent, and very luminous, events accompanied by a strong emission of gravitational waves. It is therefore the accretion disk of the black hole that makes it visible to us in many cases. But other effects may also reveal its presence, such as the jets of active galactic nuclei (AGN), the movement of stars around it, gravitational lensing effects, etc; the latter two are present even in the (academic) case of a naked invisible black hole.

An important effect is the radiation pressure exerted by the radiated photons on the falling matter: it limits the rate at which black holes can absorb matter and kind of regulates the process. As a result, a black hole of mass M cannot have luminosity in excess of some limit, called the Eddington limit, which is proportional to M. This is used to obtain a lower limit on the masses of black holes from their measured apparent luminosity and red shift (their distance being obtained from the red shift using Hubble's relation and their absolute luminosity being obtained from their apparent luminosity by scaling in proportion with the square of the distance).

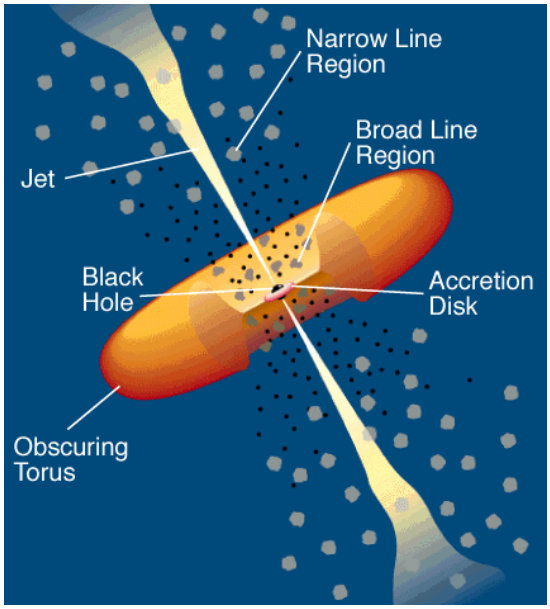

Figure 1.2: An active galactic nucleus including a super massive black hole at the centre.

It is not surprising that black holes are usually embedded in a dense environment: stellar black holes are produced as the end product of the core of a supernova

but the star envelope is ejected outwards and becomes a so-called supernova remnant (SNR). In other cases the black hole is produced in a binary system when one of its members, say a neutron star, increases its mass by collecting matter from its companion, say a red giant. We also know of so-called gamma ray bursts that have been recently studied by the SWIFT satellite, showing multiple explosions in the process leading to the creation of a black hole. Clearly such events result in a very dense environment in the region of the newly born black hole. For what concerns galactic black holes, we already said that the central region of a galaxy is densely populated as many massive objects in the galaxy slowly drift towards it. This is well known, as we shall see later, in the case of Sgr A* at the centre of the Milky Way. But there is no reason why it should be different for other galactic black holes. In the case of super massive galactic black holes the phenomenon of accretion of matter becomes so extreme that it is the source of some of the brightest objects in the sky, such as quasars.

The violence of the events implied in the creation or growth of black holes contributes to their having significant angular momentum. Such black holes, when naked, correspond to a solution of Einstein equations that was studied by Kerr, the main result being that space is kind of locked to the rotating horizon: matter falling on the black hole is dragged into a whirl around the horizon. In this movement, it tends to drift towards the equator of the horizon, pushed away by the centrifugal force, thus forming a disk (the so-called accretion disk). Clearly, the rotation velocity of the black hole cannot grow indefinitely: at some point the velocity on the equator of the horizon will reach the velocity of light, hence setting an upper limit to the rotation. However, one expects accreting black holes to reach rapidly this limit and therefore to rotate with a frequency close to the maximal permitted value.

An important factor in the description of an accreting black hole is the effect of tidal forces. Such forces exist around any star and are easily calculable in the case of a planet: consider a body of dimension d and mass m in rotation around a much heavier one (mass $M >> m$). Its centre of gravity follows a Keplerian orbit, say a circle of radius R to simplify. The average gravitational force $F = \frac{GmM}{R^2}$ is exactly balanced by the centrifugal force. But in its rest frame

it is stretched along R by a force ΔF such that $\frac{\Delta F}{F} \propto -\frac{2d}{R}$. When the tension $\frac{\Delta F}{d}$ exceeds some limit, say θ_{lim}, it causes the body to break. This limit corresponds to $\frac{2F}{R} = \frac{2GmM}{R^3} = \theta_{\text{lim}}$ or $\frac{m}{R^3} < \frac{\theta_{\text{lim}}}{2GM}$. It is called the Roche limit. For example, in the case of the moon, the Roche radius is 18 000 km compared with its actual distance to the earth, 400 000km. Conversely, at a given radius, no object having a mass in excess of the Roche mass can survive: hence the very tiny dust pieces in the Saturn rings (the mass of Saturn is ~100 earth masses, its radius is ~10 earth radii). Tidal forces around a black hole are very large at proximity of its horizon and the accretion disk is the seat of many collisions that increase its temperature. In extreme cases the temperature reaches many thousand degrees and matter is in the form of an ionized gas, with important electric and magnetic fields generated by the rotation and expelling particles along two jets along the rotation axis. Both the accretion disk and the jets, containing relativistic charged particles, emit bremsstrahlung photons that may have wave lengths going from the radio to X regions of the spectrum.

1.3. An overview of the black holes in the universe

A stellar black hole is a black hole formed by the collapse of a massive star at the end of its lifetime. When a massive star runs out of nuclear fuel, it explodes as a supernova. While the outer parts of the star are expelled violently into space, the material in the core is strongly compressed under its own weight. To create a stellar black hole, the core must have a mass in excess of two to three solar masses; the progenitor star must therefore be some 10 to 20 times more massive than our sun. This is required for gravity to overcome the nuclear pressure existing in the core of a neutron star. If the core is not massive enough, it will stay in the state of a neutron star and, if its magnetic field is strong enough, it will become a pulsar. Therefore, while there is an upper limit to the mass of a neutron star, or pulsar, there is none to that of black holes. Pulsars are characterized by their rotating beams directed along the trapped magnetic field, different from the rotation axis. This cannot happen for black holes: they cannot trap magnetic field. Therefore, the observation of a pulsar having a mass in excess of a few solar

masses, namely such that it should have become a black hole, would contradict the present theory. But all pulsars that have been observed and of which the mass has been measured have masses in only slight excess to the Chandrasekhar limit of 1.4 solar masses.

Particularly interesting has been the observation of binaries including black holes and pulsars. Cygnus X1 (Cyg X1) was the first stellar black hole to be discovered. It was first seen in 1964 as a strong X-ray emitter (the second brightest in the sky) by the team of Riccardo Giacconi, a pioneer of X-ray astronomy, using a detector in a rocket. The observation was refined using the satellite Uhuru (1971) and Giacconi got a Nobel Prize for this work. Optical and radio counterparts were observed in the early seventies. The optical observations established that Cyg X1 was a member of a binary located in the Milky Way (6 000 ly away from us), its companion being the visible star HDE 226868 (not an X-ray emitter) while Cyg X1 is invisible but is an X-ray emitter. Both have masses in excess of 10 solar masses. They are distant by only 20 solar radii from each other. The emission of X-rays from the accretion disk takes place far away from the horizon at some 10 Schwarzschild radii from the black hole. The radio observations gave evidence for radio wave bursts, simultaneous with X-ray bursts, such as one expects from turbulent hot gases around a black hole.

Here is also the place to mention the first indirect evidence for gravitational waves obtained by Joseph Taylor and Russell Hulse, a work for which they got a Nobel Prize in 1993. Using a radio telescope they found a binary made of two neutron stars (one of which is a pulsar) orbiting around each other in 8 hours. Accurate radio measurements established that they were slowly spiraling toward each other at a rate of 2.7 ppm per year. This is exactly what is predicted by general relativity as a result of gravitational wave emission. However, we should remember that no gravitational wave has been directly detected until now.

Contrasting with stellar black holes, very massive black holes are observed in the centre of galaxies. Their masses may reach many billions of solar masses. One such galactic black hole is known to exist in the centre of our own galaxy, the Milky Way. It has a mass of some three million solar masses. We shall study it in some detail in the present work. It is relatively quiet in comparison with the super massive black holes that exist in the centers of quasars, BL Lac's, Seyfert galaxies

and other active galaxies (one speaks of active galactic nuclei, AGN's). Stellar black holes interact with other stars in their galaxy and, on average, the heavier of the two – that is usually the stellar black hole – will tend to migrate toward the centre of the galaxy while the other will drift away from it. During its journey toward the centre of the galaxy, the stellar black hole will have many opportunities to grow up by swallowing matter from its environment. As a result the density of black holes – and more generally of massive stars – is important in the central region of a galaxy. The collision rate is accordingly high and the stellar black hole will ultimately merge with the galactic central black hole. This process is well understood in the (academic) case of naked black holes: what happens is that as soon as their horizons touch each other they become a single black hole, the horizon going from the topology of two separated spheres to that of a single sphere via a very asymmetric intermediary configuration. A strong emission of gravitational waves takes place during the merging process. In the case of real (dressed) black holes, the situation is not as simple, the accretion disks being first to collide, but the final result is essentially the same.

The Milky Way is some ten billion years old, so Sgr A*, on average, has absorbed some 0.3 solar masses per kyear. By contrast, a super massive galactic black hole of, say, 10^{10} solar masses must have absorbed a solar mass per year on average. Until recently, this was difficult to conceive: such super massive black holes were a puzzle to astrophysicists. Recently, however, M. Rees remarked that the nuclear chemistry that governs the evolution of stars was quite different in the very early universe that contained essentially hydrogen and helium and virtually no heavier element (we already remarked earlier that the stability, lifetime and maximal possible mass of a star were very sensitive to the detail of these reactions). He claims that a consequence is that much more massive stars could be formed in these early galaxies than in a galaxy such as ours. Wolf Rayet stars, the most massive stars in spiral galaxies such as ours, have a mass of at most 120 solar masses. In these early galaxies, according to M. Rees, star masses could have reached several thousand solar masses. Star lifetimes are shorter the heavier the star (they have a smaller core temperature and therefore a smaller number of possible reactions available to burn their hydrogen into helium). While our sun will live some 15 billion years, Wolf Rayet stars live only of the order of a million years: they explode in the same OB association where they were born; they have

no time to drift away from it. These arguments are sufficient, M. Rees claims, to explain super massive black holes as being formed from the same mechanism as other less massive galactic black holes. If this hypothesis is confirmed, super massive black holes will no longer be an enigma and it will no longer be necessary to invoke ad hoc exotic mechanisms, such as the very early production of small primordial black holes, to explain their existence and properties.

Super massive black holes are usually surrounded by very bright accretion disks, themselves embedded in a torus of opaque dust. Intense magnetic fields may be trapped in the accretion disk and, because of the rapid rotation, produce very strong electric field gradients that generate two jets of particles and radiation directed along the rotation axis. As the system is a very stable gyroscope, the direction of the jets is invariant over the very long periods during which they have been emitted.

The first such super massive black hole to have been observed is Cygnus A (Cyg A, Figure 1.3). It was first seen in 1940 as a strong radio source by Grote Reber, a radio-amateur who had assembled the first radio telescope ever built in its back yard. During the twenty years that followed, radio astronomy came of age: in 1953 R.C. Jennison and M.K. Das Gupta observed Cyg A using a radio interferometer at Jodrell Bank and resolved the two radio lobes; for some time one thought that one was dealing with two colliding galaxies but in 1963, Schmidt, Greenstein and Sandage discovered quasars and the real nature of Cyg A was finally clarified.

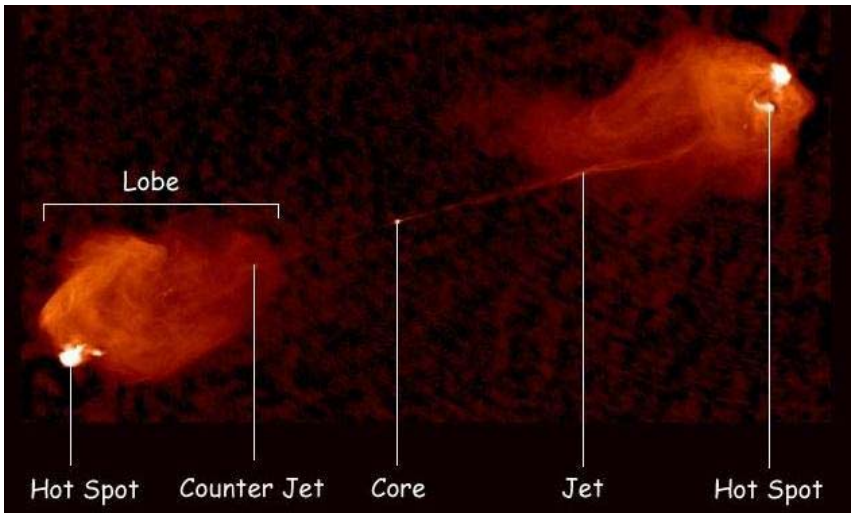

Figure 1.3: A radio image of Cygnus A

CHAPTER 2

OBSERVING THE CENTRE OF THE MILKY WAY

What we know today of the black hole located in the centre of the Milky Way is the result of many different observations. In the present section we review the methods that have been used for this purpose. As they all rely on the detection of electromagnetic radiation, namely on photon detection, we start with some elementary considerations on black body radiators, which are central to such observations.

2.1. Black body radiators

Consider a system *S* with energy levels E_n and probability $P(E_n)$ to be occupied in thermal equilibrium with a bath, or thermostat, *S'* infinitely large and having a continuous spectrum with a density of states $\rho(E')$. Thermal equilibrium implies that *S* and *S'* exchange energy but this only affects the values of $P(E_n)$ without affecting the spectrum itself, namely without changing the values of E_n. Moreover we assume that E_{tot} , the (constant) total energy of the two systems is much larger than E_n: $E_{tot} = E_n + E' >> E_n$. Then at thermal equilibrium $P(E_n)$ is proportional to $\rho(E') = \rho(E_{tot} - E_n)$. The assumption of thermal equilibrium is equivalent to the scale invariance statement $\frac{d\rho}{\rho dE'} = cte$ implying that $\rho(E')$ is proportional to $e^{-\beta E'}$ where β is a constant. We call $T = \frac{1}{k\beta}$ (where k is the Boltzmann constant, 0.086 meV/K) the temperature. The temperature is therefore defined as the energy spread over the states of the system. From $P(E_n)$ proportional to $\rho(E')$, itself proportional to $e^{-\beta E'}$, itself proportional to $e^{-\beta E_n}$ we may write $P(E_n) = \frac{e^{-\beta E_n}}{Q}$ with $Q = \sum_n e^{-\beta E_n}$.

In the case of a black body radiator we have $E_n = nh\nu$ (more precisely $(n+\frac{1}{2})h\nu$ but we can neglect the $\frac{1}{2}$) where h is Planck constant and v the frequency of the radiation. Hence the mean number of photons per unit of volume with frequency between v and $\nu + d\nu$ is

$$d\left[\frac{2\cdot\frac{4}{3}\pi\left(\frac{h\nu}{\eta c}\right)^3}{(2\pi)^3}\right] = \frac{8}{3}\pi\cdot\frac{d\nu^3}{c^3} = \frac{8\pi\nu^2}{c^3}d\nu$$

the number of phase space cells per unit volume, times

$$P(E_n) = \frac{e^{-\beta E_n}}{Q} = \frac{1}{e^{\frac{h\nu}{kT}} - 1}$$

From this we get the black body radiation spectrum: A black body at temperature T radiates, per unit area, a power P that depends upon frequency as given by Planck's law:

$$\frac{dP}{d\nu} = -\frac{2hc^{-3}\nu^3}{e^{\frac{h\nu}{kT}} - 1}$$

Taking the derivative with respect to the wave length $\lambda = \frac{c}{\nu}$ gives the Wien's laws:

$$\lambda_{\max}(\mu m) \approx \frac{2900}{T}$$

and

$$T^{-5}\frac{dP}{d\lambda} \approx 8\pi\ \mu W m^{-3} K^{-5}$$

at maximum emission. Integrating instead over λ gives the Stefan-Boltzmann law, $T^{-4}P = 5.7\times10^{-12} W cm^{-2} K^{-4}$. Developing to first order Planck's law in ν gives

$$\frac{dP}{d\nu} = -\frac{2hc^{-2}\nu^3}{\frac{h\nu}{kT}} = -\frac{2kT}{\lambda^2}$$

the Rayleigh-Jeans relation. Wien's law relates the wave length at maximum to temperature, 1μm (visible) corresponding approximately to 2900 K, 10μm (infrared) to 290K, 1mm (CMB) to 2.9K, 1cm (radio) to 290mK. The table below summarizes these results. Note that Wien's law relates the black body temperature T to the wave length at maximum which differs from a simple multiplication by Boltzman constant.

	$\lambda_{max}(m)$	$\nu_{max}(Hz)$	$E_{max}(eV)$	$T_{max}(K)=E_{max}/k$	*T(K) from Wien's law*
Radio	1	$3\ 10^{8}$	$1.2\ 10^{-6}$	$1.4\ 10^{-2}$	$2.9\ 10^{-3}$
Radio/μwave	10^{-2}	$3\ 10^{10}$	$1.2\ 10^{-4}$	1.4	0.29
μwave/IR	10^{-4}	$3\ 10^{12}$	$1.2\ 10^{-2}$	$1.4\ 10^{2}$	29
IR/visible/UV	10^{-6}	$3\ 10^{14}$	1.2	$1.4\ 10^{4}$	$2.9\ 10^{3}$
UV/X	10^{-8}	$3\ 10^{16}$	$1.2\ 10^{2}$	$1.4\ 10^{6}$	$2.9\ 10^{5}$
X/γ	10^{-10}	$3\ 10^{18}$	$1.2\ 10^{4}$	$1.4\ 10^{8}$	$2.9\ 10^{7}$
γ	10^{-12}	$3\ 10^{20}$	$1.2\ 10^{6}$	$1.4\ 10^{10}$	$2.9\ 10^{9}$
γ	10^{-14}	$3\ 10^{22}$	$1.2\ 10^{8}$	$1.4\ 10^{12}$	$2.9\ 10^{11}$

2.2. Radio astronomy

Radio waves are the electromagnetic waves that have the longest wave lengths, from 1 mm to 100 m. Above 100 m they are reflected by the ionosphere and cannot reach the earth. In space, beyond the ionosphere, one could in principle (for example on the moon) detect radio waves up to 10 km wave length. Many astronomical objects emit radio waves. The first radio astronomical observations were made in 1932 by Karl Jansky, a Bell Lab physicist who detected cosmic radio noise from the Milky Way while investigating radio disturbances interfering with transoceanic communications. Since then, astronomers have built many radio

telescopes with sophisticated systems that allow for a high angular resolution resulting in the production of detailed radio pictures of celestial objects.

Radio telescopes all have two basic components: a large radio antenna (or set of antennas) and sensitive radio receivers. As an example, the Very Large Array (VLA) is one of the world's best astronomical radio observatories (Figure 2.1). It consists of three equal arms of 9 antennas each, symmetrically arranged at 120^{o} from each other. The antennas are parabolic, 25 m in diameter and the array is 36 km across.

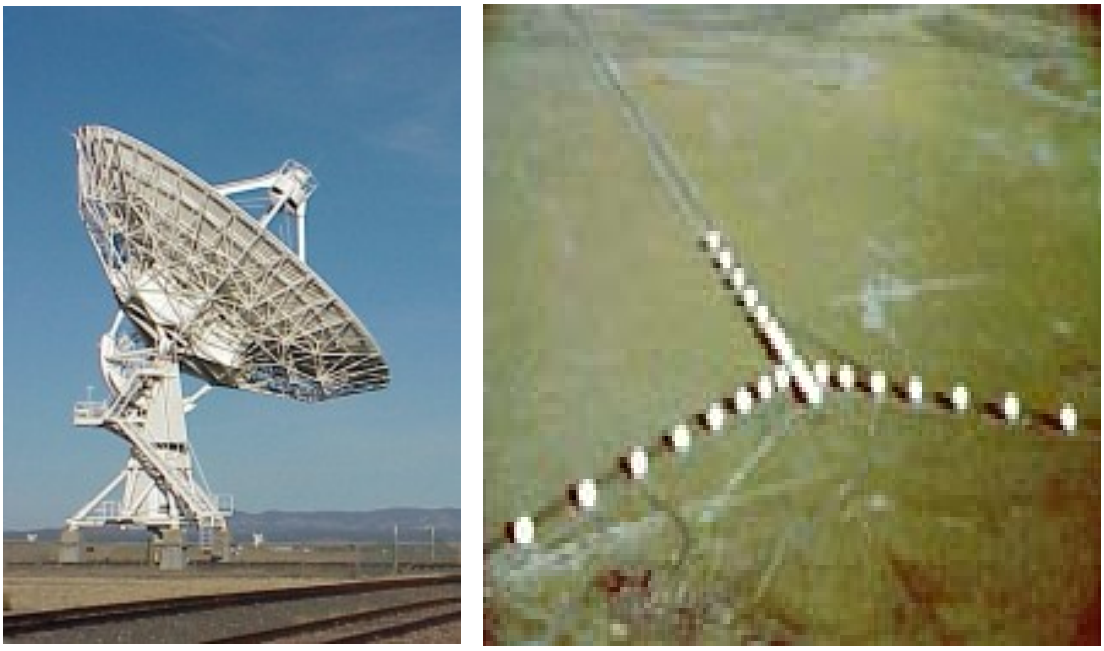

Figure 2.1: An antenna of the VLA (left) and the VLA array (right).

Incoming signals are collected by the dish of the antenna and reflected by its parabolic surface to the focus called the “knobby widget” where there is either another reflector (as in the VLA) or a receiver. In the VLA the focal reflector is movable and can, at will (according to wave length), send the signal back to one of several waveguide terminals located in the centre of the dish. From there it is transferred to the receivers that are located below the antenna and cooled down to 15 K in order to minimize thermal noise. The receiver amplifies separately the two opposite circular polarizations components of the signal.

Differential fluxes (fluxes per unit of frequency) are measured in Jansky ($=10^{-26} W/m^2/Hz$). When the flux has its source in thermal emission, the frequency spectrum is that of a black body with a Planck distribution. In the case of radio waves, where one is dealing with large wave lengths, the Planck relation reduces to the so-called Rayleigh-Jeans relation: the flux Φ is related to the black body temperature T through the relation $\Phi = \frac{2kT}{\lambda^2}$ where k is the Boltzman constant and λ the wave length. The lowest temperature that can be detected is limited by the detector thermal noise and is equal to $T_{\min} = \frac{T_s}{\sqrt{B\tau}}$ where B is the bandwidth, τ the time of integration and T_s the temperature of the receiver. The lowest detectable flux is therefore $\frac{2kT_{\min}}{\lambda^2}$. In practice, one can go down to $T_s = 10K$.

The sensitivity of a radio telescope, the ability to measure weak sources of radio emission, is proportional to the area and efficiency of the antenna and the sensitivity of the radio receiver used to amplify and detect the signal. For broadband continuum emission the sensitivity also trivially depends on the bandwidth of the receiver.

The angular resolution, or ability of a radio telescope to distinguish two neighbor sources, namely fine details in the sky, is limited by diffraction: it is equal to the ratio between the wavelength of observation and the diameter of the antenna of the instrument. This is at variance with ground observation in the visible where it is atmospheric turbulences (changing the index of refraction) rather than diffraction that limit the angular resolution. For a same angular resolution a short wave length antenna will therefore afford to be smaller than a large wavelength antenna.

Radio waves penetrate much of the gas and dust in space as well as the clouds of planetary atmospheres and pass through the terrestrial atmosphere with little distortion. In principle, radio astronomers can therefore obtain a much clearer picture of stars and galaxies than is possible by means of optical observation from ground. However this requires the use of very large antennas.

The first big parabolic antenna was built in Jodrell Bank (United Kingdom) in 1957 (Figure 2.2). It has a diameter of 75m and detects wave lengths larger than 15cm. The largest movable parabolic antenna ever built is 100m in diameter and is located in the Eiffel Mountain (Germany) near Bonn. In1963 Cornell University built a fixed antenna in Arecibo (Porto Rico). It is 305 m in diameter and is installed in a natural basin (Figure 2.3). It is made of a metallic grid resting on cables and the receiver, hanging 150m above ground, can move around by $\pm 20^{o}$.

Figure 2.2 The Jodrell Bank antenna in the United Kingdom is 75 m in diameter.

Building significantly larger antennas is not possible: thermal deformations and, more importantly, mechanical deformations in the case of a movable antenna, distort the shape of the detector beyond the permissible limit, i.e. a fraction of a wave length – typically one tenth.

However, interferometry allows for much better angular resolutions: having two antennas far apart is the same as having two small distant pieces of a very large antenna as far as angular resolution is concerned (but of course, as far as sensitivity is concerned, it is not: the only way to increase the sensitivity is to

increase the size of the receptor or to lower T_{min}). This is the idea of interferometry which implies that the two antennas, distant from each other, are positioned to better than a fraction of a wavelength (as they should be if they were part of a same reflector). In practice this is done by looking at the interference pattern between the two receivers. Such arrays of antennas have been built in several sites around the world and the VLA is the best such example. One can even, in principle, have antennas separated by as much as an earth diameter. Indeed networks of such antennas exist and the data are recorded together with the time given by an atomic clock and are combined later on in a computer.

Figure 2.3. Aerial view of the Arecibo antenna in Porto Rico

Radio sources can produce radio waves by thermal emission (usually resulting from the thermal movement of electrons and ions in a plasma) or by non thermal emission (such as synchrotron radiation or coherent movements in oscillating plasmas).

Thermal emission obeys the Rayleigh Jeans relation. Planets have their maximum of emission in the infrared. Interesting information is obtained from a comparison of their temperatures measured with radio waves or with infrared

radiations. For example Venus is found to be at 600K by radio and at 225 K by infrared. The reason is the clouds that surround it and the green house effect that results. Radio waves probe the surface of the planet while infrared radiation probes the clouds. In situ measurements have confirmed these results. Outside of the solar system radio waves are good detectors of gas clouds in the interstellar matter, of supernova remnants and of plasmas of various kinds. In particular, electron-proton collisions at large impact parameters produce what is referred to as free-free emission.

When an electron (charge e and mass m) moves in a magnetic field H at a velocity β with respect to the light velocity, it follows an helix and emits synchrotron radiation, namely photons having a so-called Larmor frequency $f = \frac{eH}{2m\sqrt{1-\beta^2}}$. The maximum of the synchrotron emission is at a frequency $f(MHz) = 0.5 \times 10^{-7} E(eV)^2 H(T)$. This mechanism, together with coherent plasma oscillations, is the main source of non-thermal emission.

In addition to these continuous spectra there are also line spectra in radio astronomy as there are in the visible. The most famous is the 21cm hydrogen line (corresponding to the spin-flip of the electron of a neutral atom). But there also exist many other molecular lines that tell us which molecules are present in interstellar clouds. Moreover, line spectra allow for a measurement of the velocity of the object from their Doppler shift.

One should also mention that the polarization of the radio wave provides information on the magnetic field in the radio source and/or the magnetic field in clouds located between the source and the earth.

2.3. Infrared, visible and ultraviolet astronomy

For many centuries astronomy was based exclusively on observations in the visible part of the electromagnetic spectrum. As we just said, the last century saw the birth of radio astronomy with observations typically in the millimeter to decimeter range. These are indeed the only two frequency windows that are not significantly absorbed by the Earth atmosphere. As shown in Figure 2.4 the atmosphere absorbs completely the other wavelengths. They could only be

observed when space astronomy made it possible in the second half of the past century.

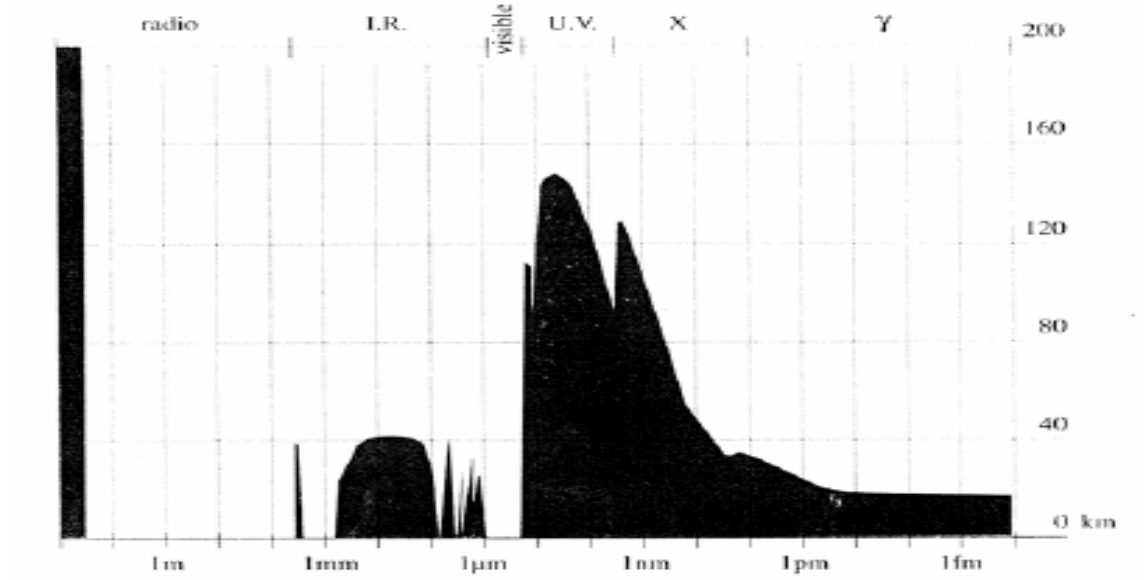

Figure 2.4 : The altitude (in km) at which one has to climb to observe electromagnetic radiations without significant attenuation as a function of their wavelength. The visible window separates the radio, microwave and infrared regions on the left from the ultraviolet, X and gamma regions on the right.

The visible window and the nearby parts of the infrared and ultraviolet frequencies can be observed from Earth where very large diameter telescopes are operated. The main component of a telescope is its mirror that reflects the light to its focus where it is reflected a second time to light detectors located outside the mirror (through a hole in the centre, just behind the reflecting surface). Different designs aimed at minimizing possible aberrations (mostly geometric, very little chromatic) are being used. The most common are a parabolic main mirror with a hyperbolic reflector (Cassegrain and Ritchey-Chrétien) or a spherical main mirror equipped with a correcting lens at its centre of curvature (Schmidt).

Today, the naked eye and photographic plates have been replaced by electronic detectors structured in pixel arrays that make it possible to record the data in large scale memories. Most of what was said for radio astronomy remains valid here: the sensitivity is proportional to the mirror area, space resolution is proportional to the ratio of the wavelength to the mirror diameter, and

interferometry makes it possible to increase it by very large factors. However, at variance with radio astronomy, observations in the visible are not diffraction limited but are limited by turbulences in the atmosphere. To be free of this constraint one may either go to space, as is the case of the Hubble Space Telescope (HST, Figure 2.5), or use corrective optics as will be described below. There exist many ground telescopes that operate in the visible and only a few orbiting the Earth, the main one being the HST. Space telescopes do not suffer from absorption or distortions in the Earth atmosphere. Their operating range depends only on their optics. The HST can observe between 0.11

Figure 2.5. The Hubble Space Telescope

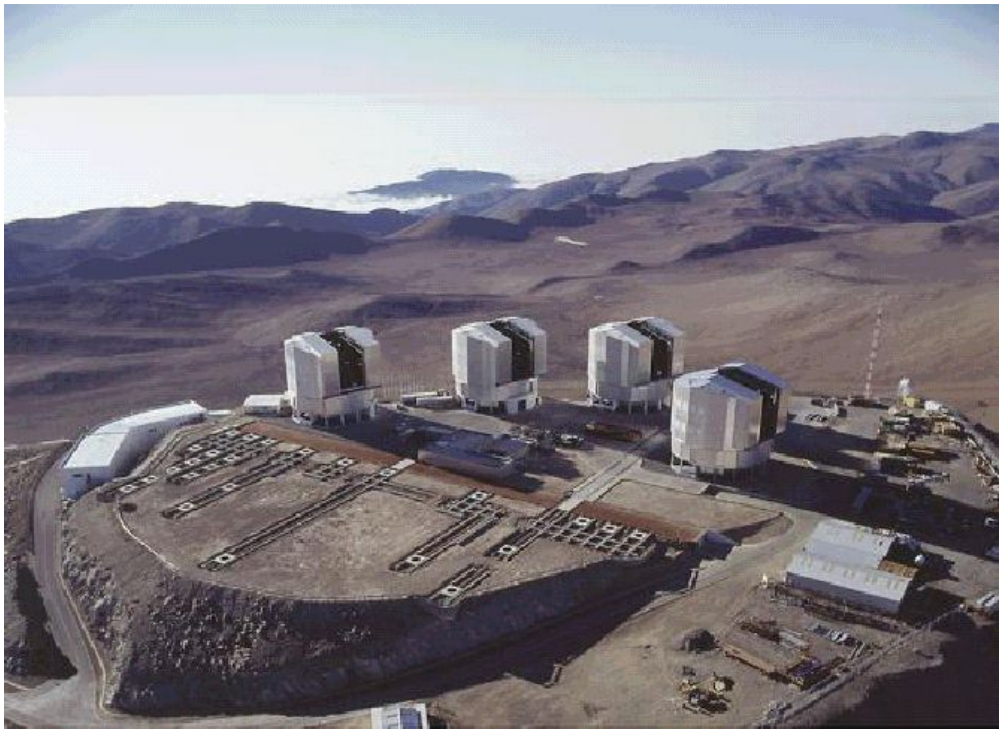

Figure 2.6. The Very Large Telescope array

and 1.1 μm, a spectral range that includes both the near infrared and the near ultraviolet region.

The Very Large Telescope (VLT) is a set of four telescopes operated by the European Southern Observatory (ESO) in La Silla (Chile), each having a 8.2 m diameter mirror (Figure 2.6). They can be operated independently or together (in which case they are equivalent to a 16 m diameter telescope in terms of sensitivity) or in an interferometer mode in order to reach very high angular resolutions. They are sensitive to a wavelength range extending from the near UV up to 25 μm in the infrared.

In the UV range, the Ultraviolet Imaging Telescope (UVIT, figure 2.7) is a 38 cm Ritchey-Chrétien telescope equipped for ultraviolet filter and grating imagery over a 40 arc minute field of view with a resolution of 3 arc sec, much better than that of HST, and covering the 120 to 300 nm wavelength range. When the field of view is reduced to 2.5 arc minute a resolution of 0.1 arc sec can be reached. Among the space ultraviolet telescopes we may mention the International Ultraviolet Explorer (IUE) that has been operating from 1978 to 1996. It was installed aboard a spacecraft of the Indian-Canadian ASTROSAT mission together with an X-ray telescope.

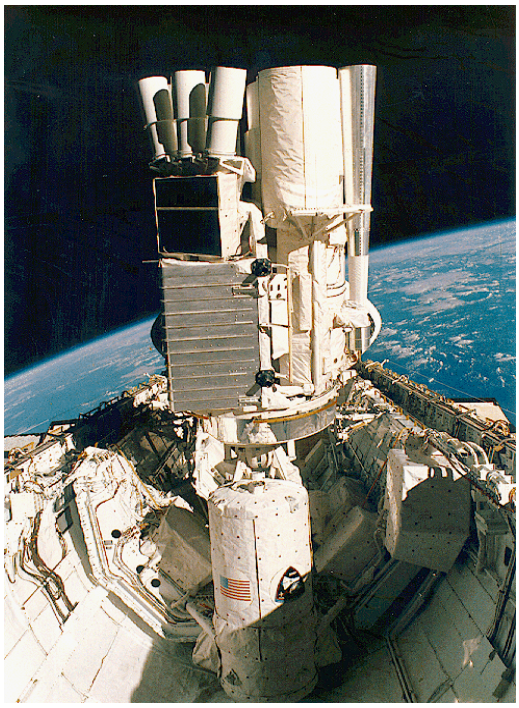

Figure 2.7: The Ultraviolet Imaging Telescope

The centre of the Milky Way is surrounded by clouds of dust that make its observation in the visible very difficult. However, a major contribution to the study of its central black hole has been made in the infrared on the VLT using the Coudé Near Infrared Camera (CONICA, Figure 2.8) on YEPUN, one of the four VLT telescopes.

Because of the importance of this observation we devote some lines to its description.

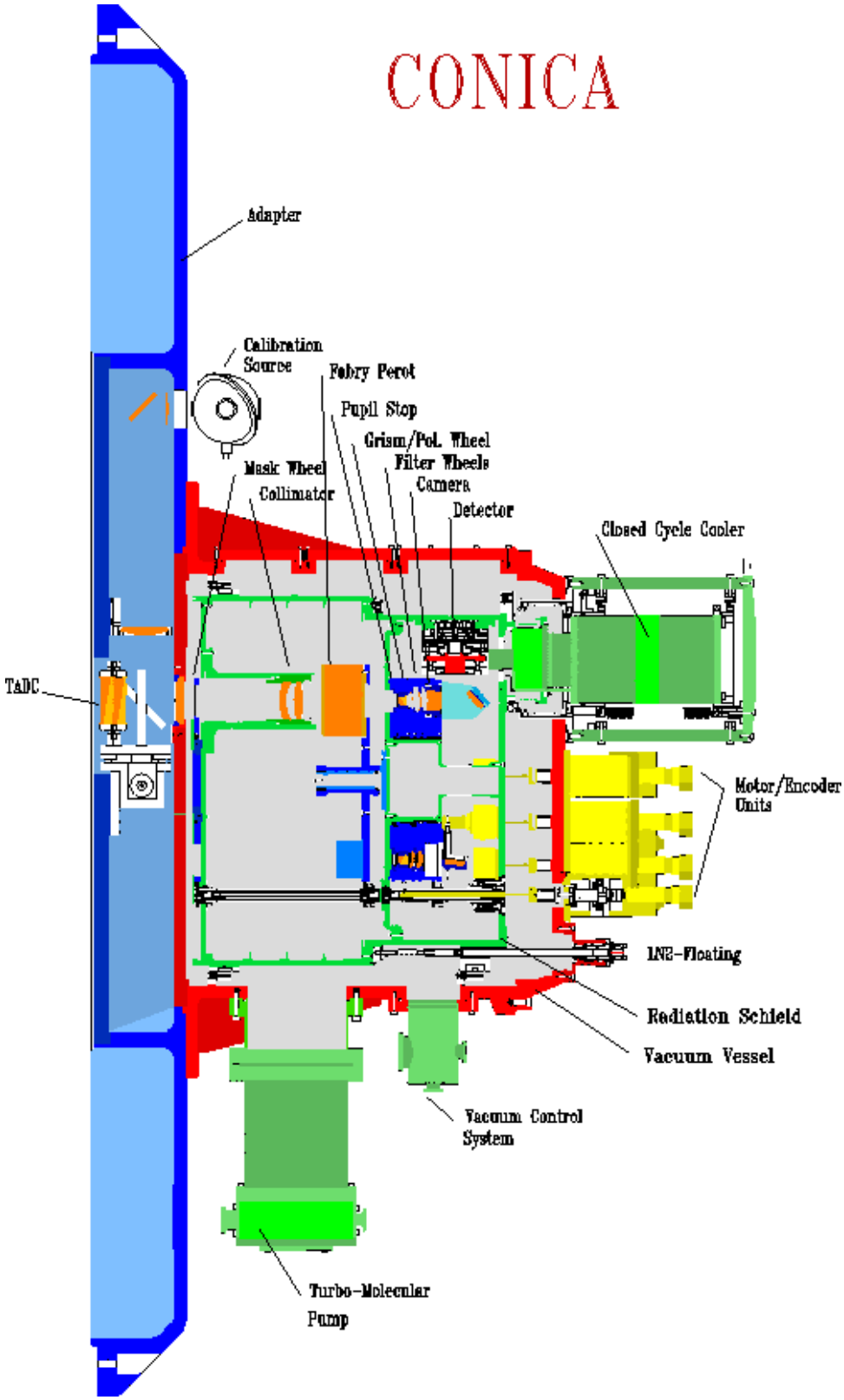

Figure 2.8: The CONICA camera.

Observation in the near infrared is very similar to observation in the visible. Essentially, all what needs to be done is to use lenses and mirrors that are transparent to infrared and detectors that have their maximal response in that spectral region. Detectors use HgCdTe or InSb pixels. Optical elements may use special glasses in the near infrared (normal glasses are transparent up to 2.8μm but special glasses such as As_2S_3 or As_2Se_5 exceed 5 μm) or, in the far infrared, semi conductors such as Si or Te or, better, gallium arsenide that is transparent between 1 and 15 μm. However the latter materials have very high refraction indices and must be coated with thin intermediate refractive index layers in order to reduce reflections. The reason that makes infrared observation of the Sgr A region easier in the near infrared than in the visible is that there are too many sub-micron dust grains in the centre of the galaxy, which make an opaque veil in the visible but not in the infrared. CONICA is installed at the VLT YEPUN Unit Telescope (UT4) (Figure 2.6) and operates in the 1 to 5μm spectral range. It uses a 256×256 HgCdTe pixel array for the 1-2.5μm wavelength range, and a 1024×1024 InSb pixel array for the 1-5μm range. It is operated at about 80K, the detector array is cooled down to 35K, all optical components are located inside the cryostat.

What makes the originality of this instrument is the use of an adaptive optics that corrects fully for the aberrations due to the fluctuations of the air refractive index caused by turbulences in the atmosphere. The adaptive optics system that equips CONICA is called NAOS (for Nasmyth Adaptive Optics System, Figures 2.9 and 2.10). The principle of the method (Figure 2.11) is to use a flexible mirror that can be deformed very rapidly (faster than the characteristic frequency of atmospheric turbulences). A reference star located within 55 arc seconds of the object under study is used to this end. Its magnitude should be less than about 17 in the visible and less than about 13 in the infrared K band. Part of the light collected in the telescope is deviated by a dichroic plate toward a pixel array through a corresponding array of micro-lenses, each micro-lens focusing the image on the associated pixel. The flexible mirror – a reflective membrane stretched on a circularring – is deformed in such a way to bring the reference star image in the centre of each pixel. The necessary deformations are determined by a simple algorithm. In some cases, they are made electrostatically using one electrode for each pixel but in the case of NAOS they are made using 185 piezoelectric fingers that can stretch over 10 μm with a precision of 30 nm. An

Figure 2.9. NAOS–CONICA at the VLT. From left to right: the telescope adapter (dark blue), NAOS (light blue), and the CONICA cryostat (red). The control electronics is located in the white cabinet.

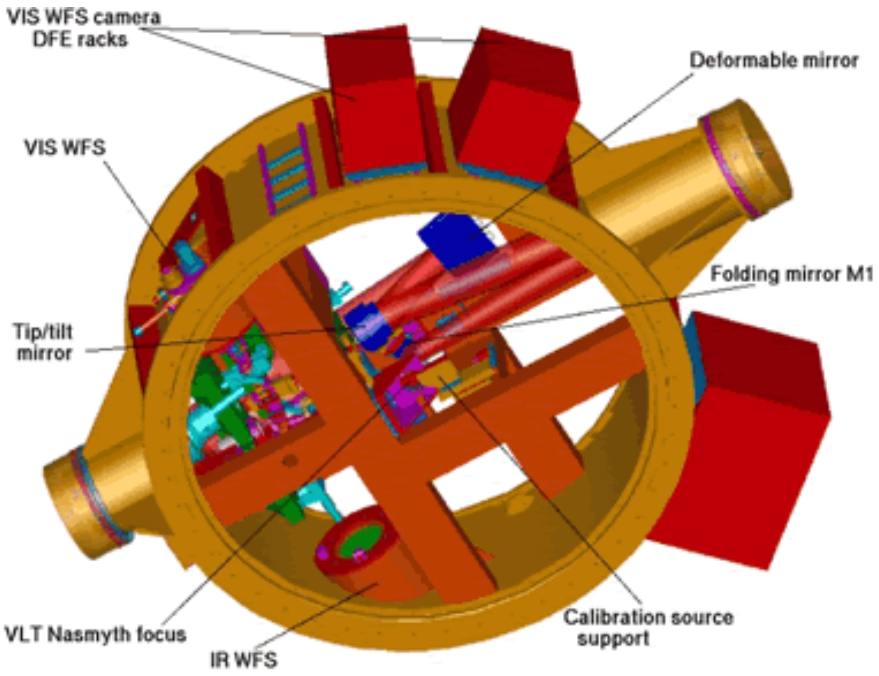

Figure 2.10: Schematic assembly of the NAOS components.

additional mirror, the tilt-tip mirror, is used to centre the image globally. The field of view (diameter) varies between 14 arc sec for the largest magnification and 73 arc sec for the smallest magnification. NAOS uses two wave front sensors, one in the visible and one in the near-infrared spectral range. The whole operation can be performed much faster than the time over which the atmosphere changes its configuration and the correction can therefore be made on line, producing an image free of turbulence aberrations and of a quality as good as if it had been made from space. One speaks of diffraction limited imaging (meaning not turbulence limited imaging as is normal for observations in the visible). Figures 2.12 to 2.15 illustrate the kind of improvement achieved.

Finally it should be mentioned that VISTA (Visible and Infrared Survey Telescope for Astronomy) is a new 4m wide field survey telescope currently under development which will be the world-leading facility in the infrared spectral range.

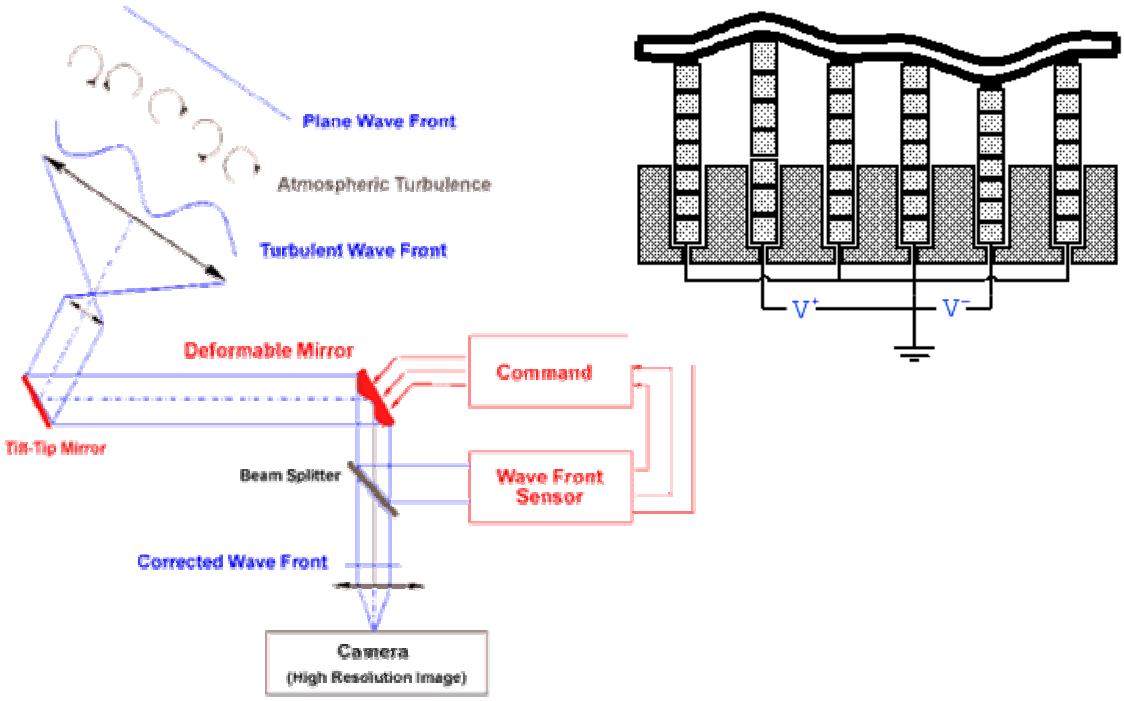

Figure 2.11: Principle of adaptive optics system with a principle drawing of the deformable mirror in the upper right corner.

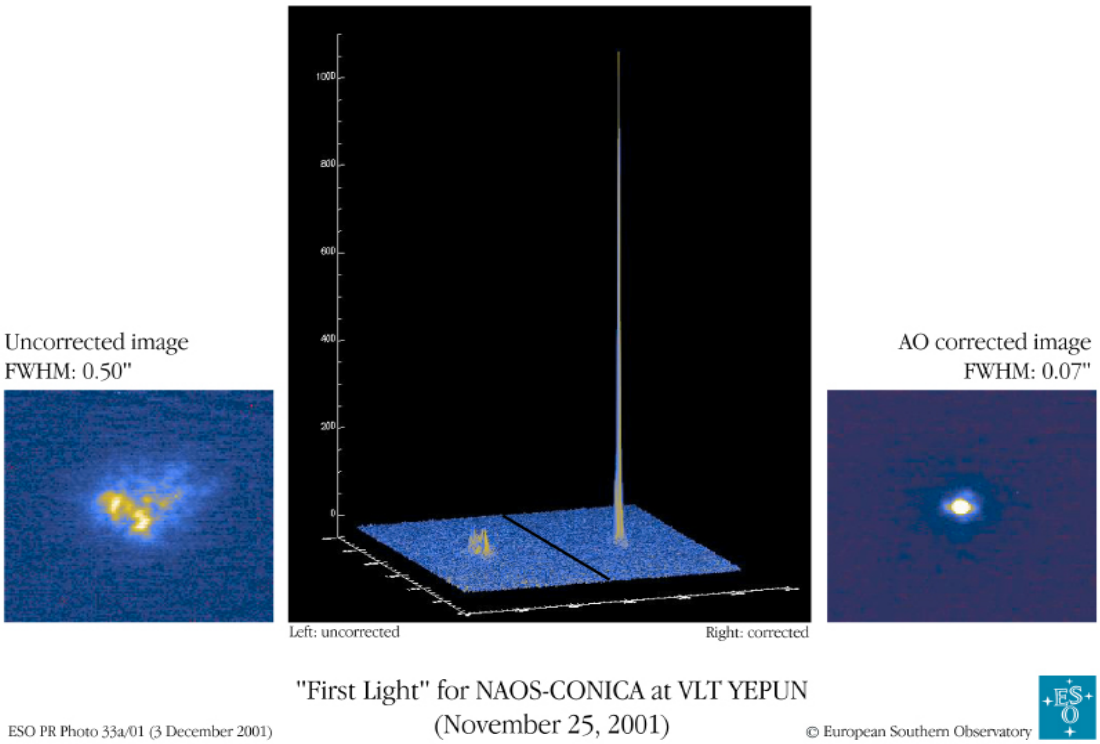

Figure 2.12: The first image in the infrared K-band of a star before (on the left) and after (on the right) using NAOS

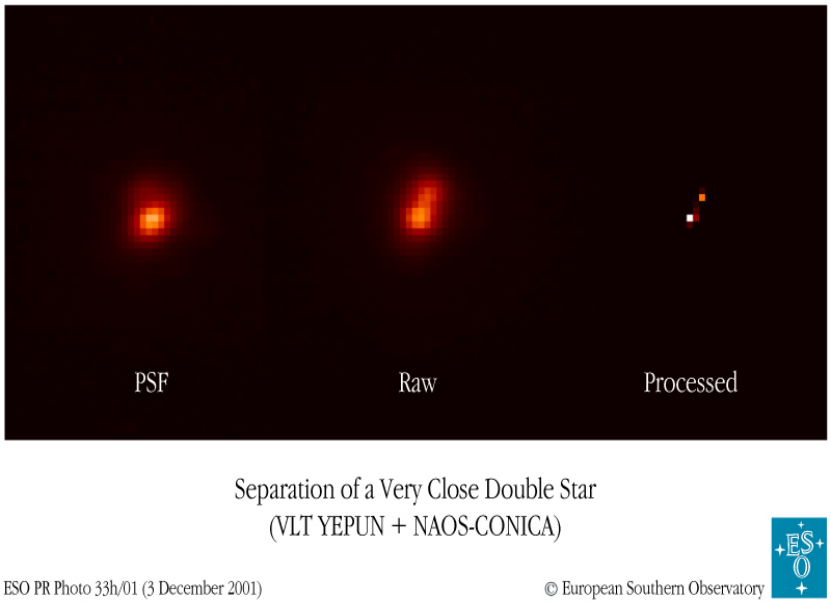

Figure 2.13: NAOS-CONICA image of double star GJ 263 with angular separation of only 0.03 arcsec. The raw image in the middle is compared to the NAOS image on the right. The Point-Spread-Function (related to the reference star) is shown on the left.

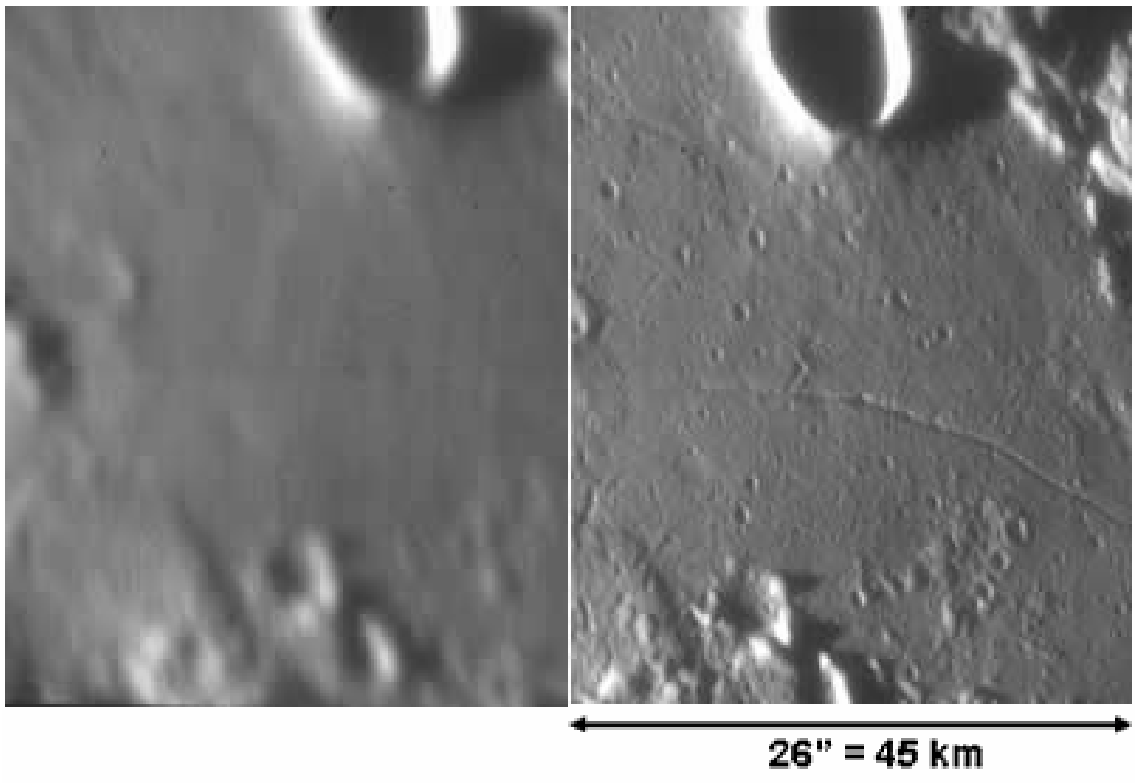

Figure 2.14. An infrared image of the moon before and after correction by NAOS

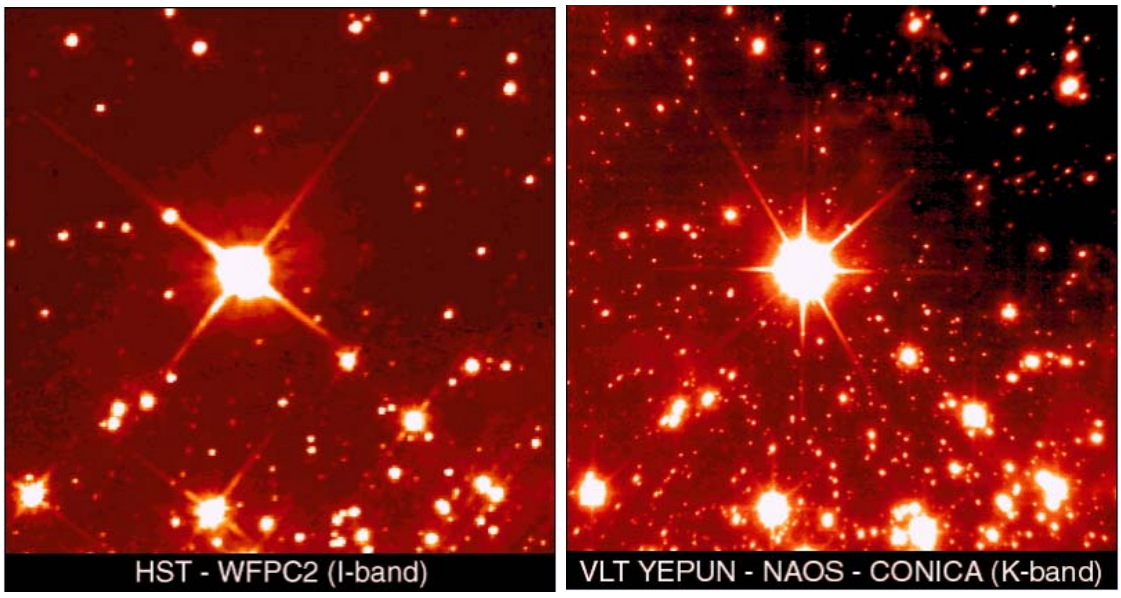

Figure 2.15 : A comparison between two images of starburst cluster NGC 3603, one obtained with the WFPC2 camera on HST in I-band and the other with NAOS-CONICA in K-band.

2.4 X-ray astronomy

Photons become more and more absorbed when their frequency increases. Already in the UV range it is necessary to use special materials having a reasonably good transparency such as quartz or fluorine. But for wave lengths shorter than 100 nm there exist no material sufficiently transparent to build conventional optical systems. What is done then, in the far UV and the soft X-ray ranges, is to use grazing incidence optics. This takes advantage of the fact that all materials have an index of refraction very slightly lower than unity in this frequency range. This implies that there is total reflection at grazing incidence, the critical angle being of the order of 1^o for 1 keV photons. However it decreases rapidly when the energy increases and above 5 keV or so grazing incidence optics can no longer be used. One then relies on complex arrangements of collimators to measure where the photons come from. One advantage of grazing incidence optics is that it allows for several coaxial parabolic or hyperbolic mirrors to be used simultaneously, as the light stays very close to the mirror surface. This is the case in CHANDRA (Figure2.16) which uses four pairs of mirrors nested into each other (Figure 2.17).

The mirrors focus the X-ray photons onto detectors which record their number, position, energy, and time of arrival.

The High Resolution Camera (HRC, Figure 2.18) includes two micro-channel plates installed at the focus of CHANDRA and can reveal details as small as one-half of an arc second. Micro-channel plates (Figure 2.19) are made of millions of very tiny lead glass tubes (69 millions of 10 μm in diameter and 1.2 mm long tubes in the HRC case) packed against each other between two flat electrodes providing an electric field of several kV/cm. The inner surfaces of the tubes are coated with a material having a large photo-electric emission, similar to the photocathode of photomultiplier tubes. When a photon hits such a surface the generated photoelectrons bounce on the walls of the tube, generating each time new photoelectrons and at the exit of the tube one finds an ensemble of accelerated electrons having large enough a charge to be easily detected and measured. The energy can be measured by using grazing incidence deflectors acting as prisms do on visible light or by replacing the micro-channel plates by charged-coupled devices (CCD) that are energy sensitive.

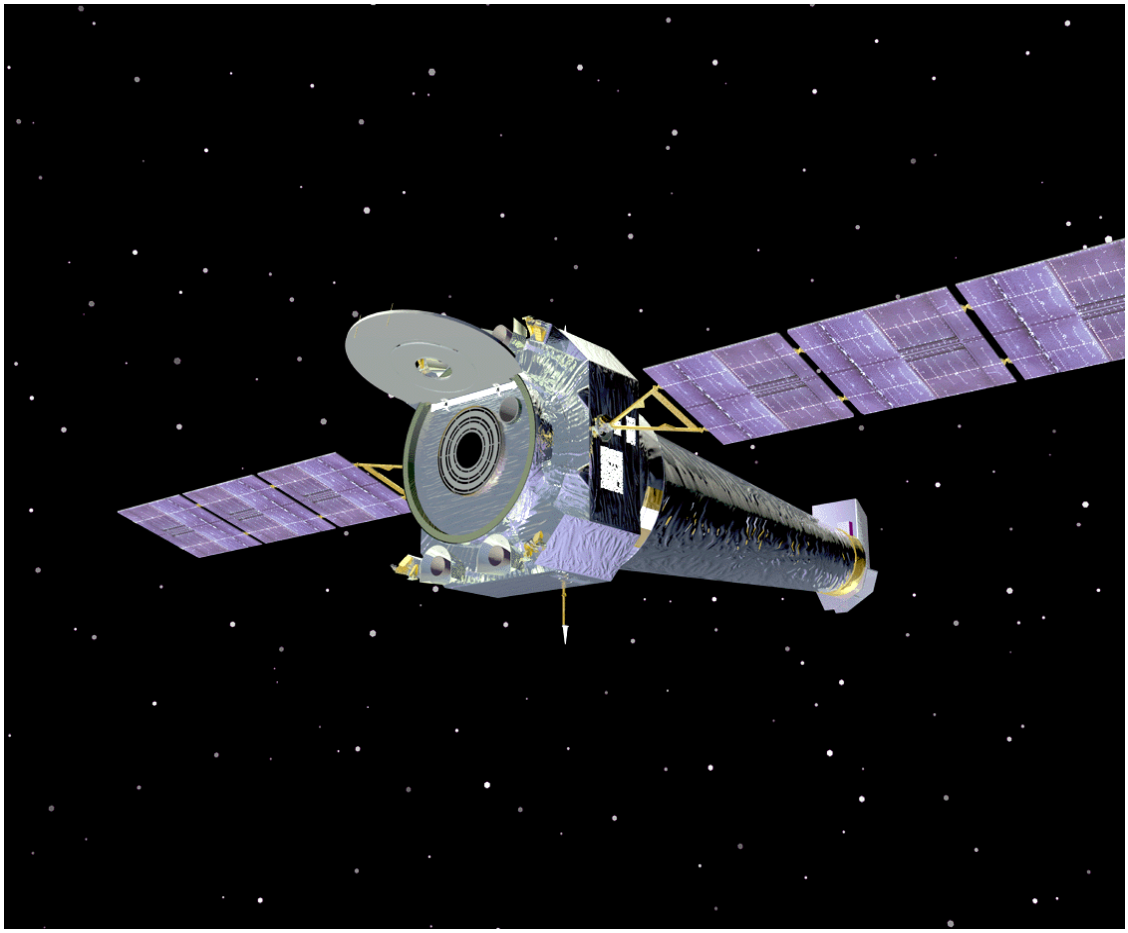

Figure 2.16 An artist view of CHANDRA showing the uncovered entrance face of the mirror system.

X-ray astronomy is useful in revealing thermal or synchrotron sources of high energy electrons. A spectacular example is shown in Figure 2.20. This composite X-ray (blue)/radio (pink) image of the galaxy cluster Abell 400 shows radio jets immersed in a vast cloud of gas that pervades the cluster. This hot gas, at a temperature of several million degrees, emits X-rays. The jets emanate from the vicinity of two super massive black holes (bright spots) in the dumbbell galaxy NGC 1128 which has produced the giant radio source, 3C 75. The peculiar dumbbell structure of this galaxy is thought to be due to two large galaxies that are in the process of merging. The discovery of the presence of important amounts of hot gas in galaxy clusters, accounting for most of the missing 3% of baryonic matter in the universe, is a major success of X-ray astronomy.

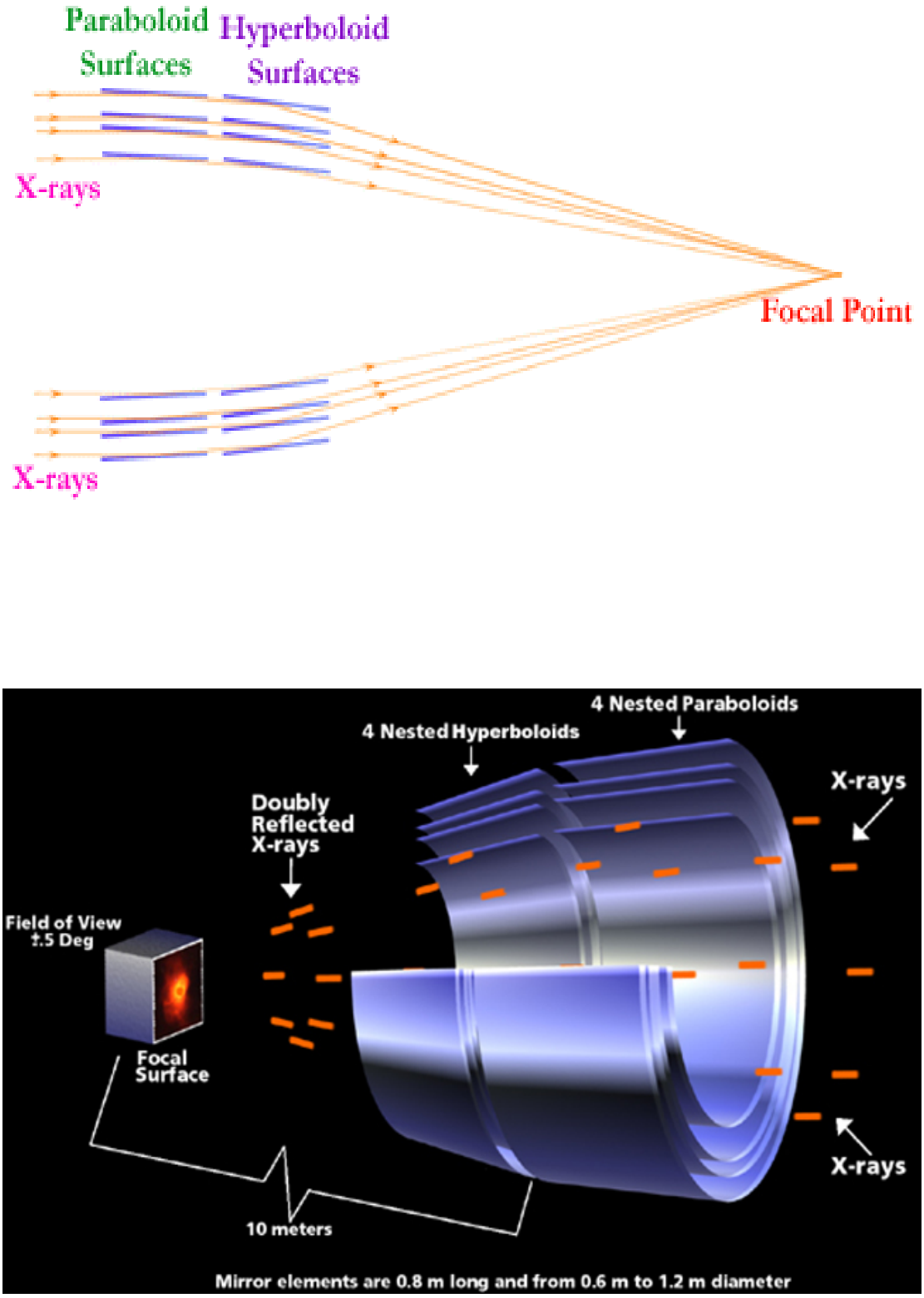

Figure 2.17: Principle of the focusing optics of CHANDRA.

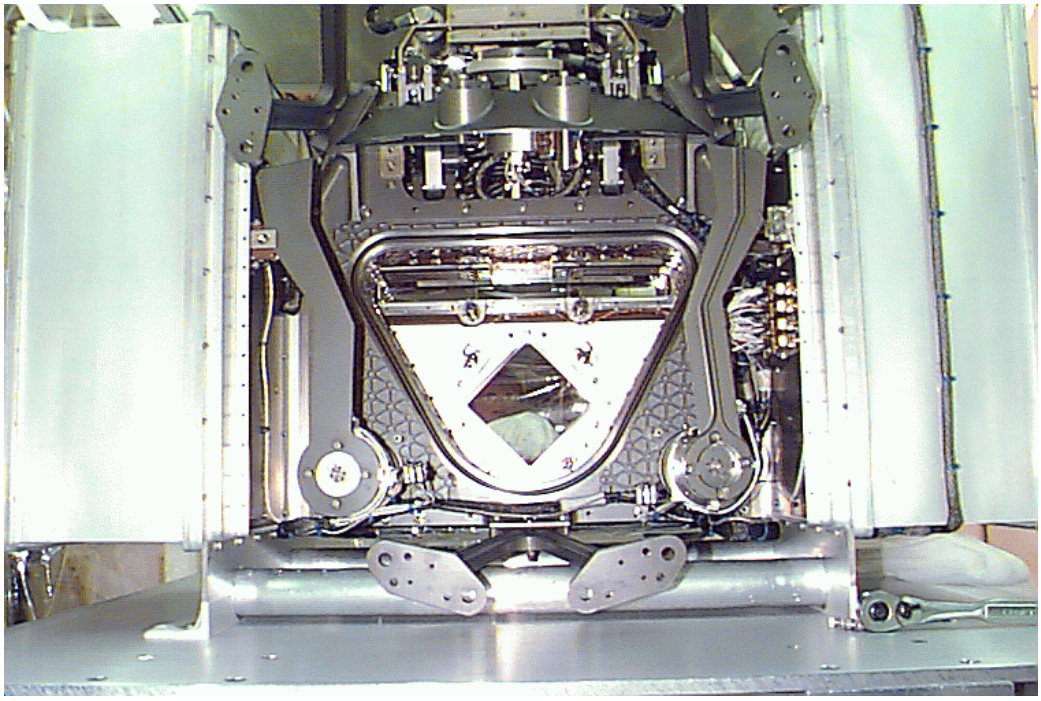

Figure 2.18: The CHANDRA High Resolution Camera

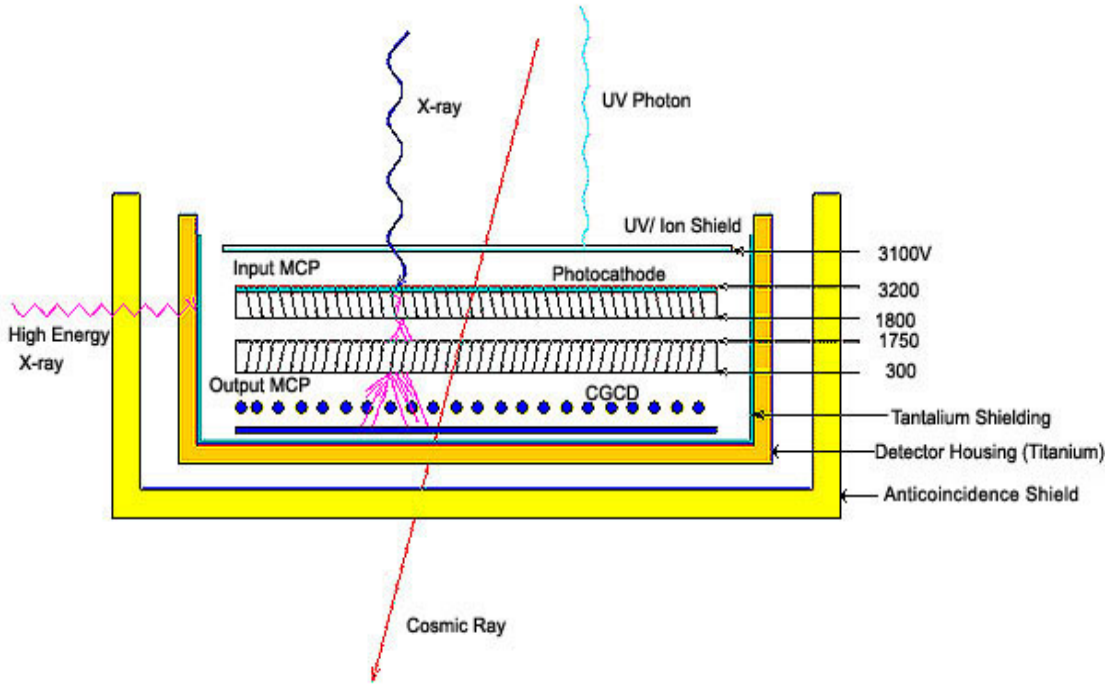

Figure 2.19. Principle of micro-channel plate (MCP) detection of X-rays (see text). The detector is protected from background radiation by shields and anticoincidence counters.

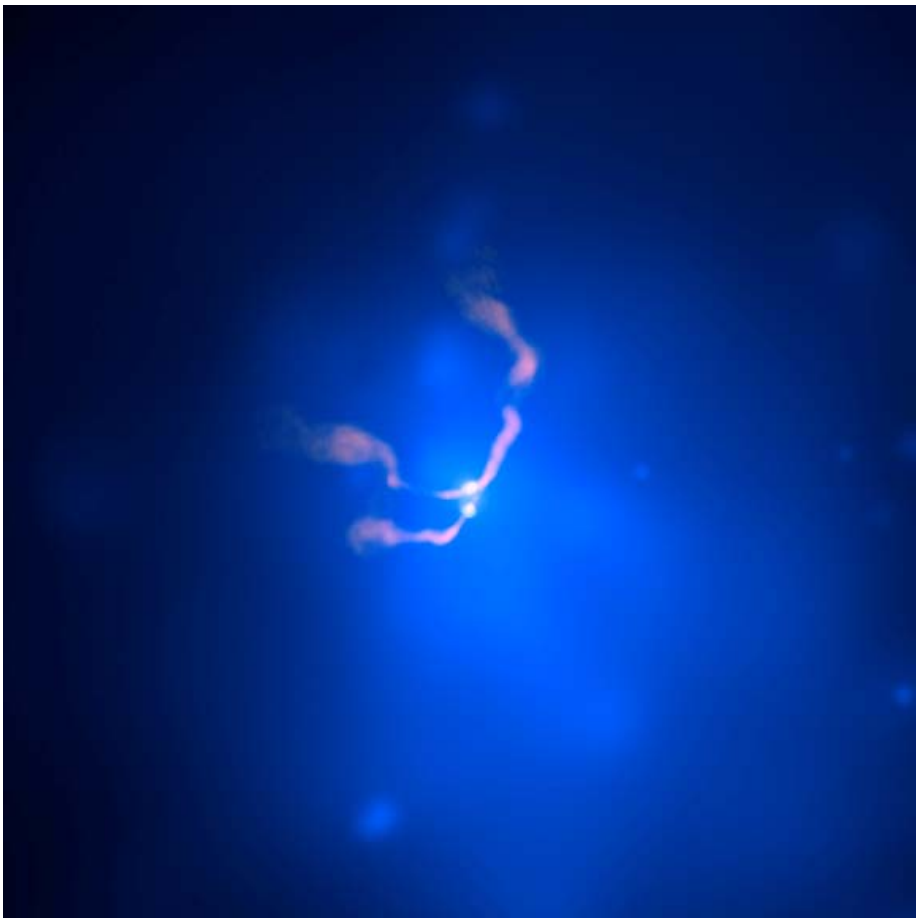

Figure 2.20. The dumbbell galaxy NGC 1128 (see text).

2.5 Gamma ray astronomy

Gamma ray astronomy in space has been active for several decades, using detectors similar to and extrapolated from those used for X-ray astronomy, in particular relying on complex arrangements of collimators to locate the detected gamma ray and to measure its direction. Today, a particularly active branch of gamma ray astronomy in space is devoted to the study of gamma ray bursts.

But at higher energy, where the rates are very low, space detectors have too small an acceptance to be sufficiently sensitive. One has then to return to ground observations, this time using the Earth atmosphere as a detector. Research in this domain is relatively recent and is progressing rapidly. As it is intensively used to observe the galactic centre, we devote a few lines to its description. Ground gamma ray astronomy detects the Cherenkov light produced by the electrons and

positrons contained in the electromagnetic shower induced by the cosmic photon in the Earth atmosphere. When an incoming high energy gamma ray enters the atmosphere, it generates a shower of particles, photons, electrons and positrons, the former being essentially produced by bremsstrahlung and the latter by pair creation. This shower (Figure 2.21), as long as the incident photon is of not too large an energy, is confined to the top of the atmosphere and can therefore be separated[2] from the hadronic showers produced by cosmic rays (nuclei) which extend down to lower altitudes. Most electrons (and positrons) are strongly

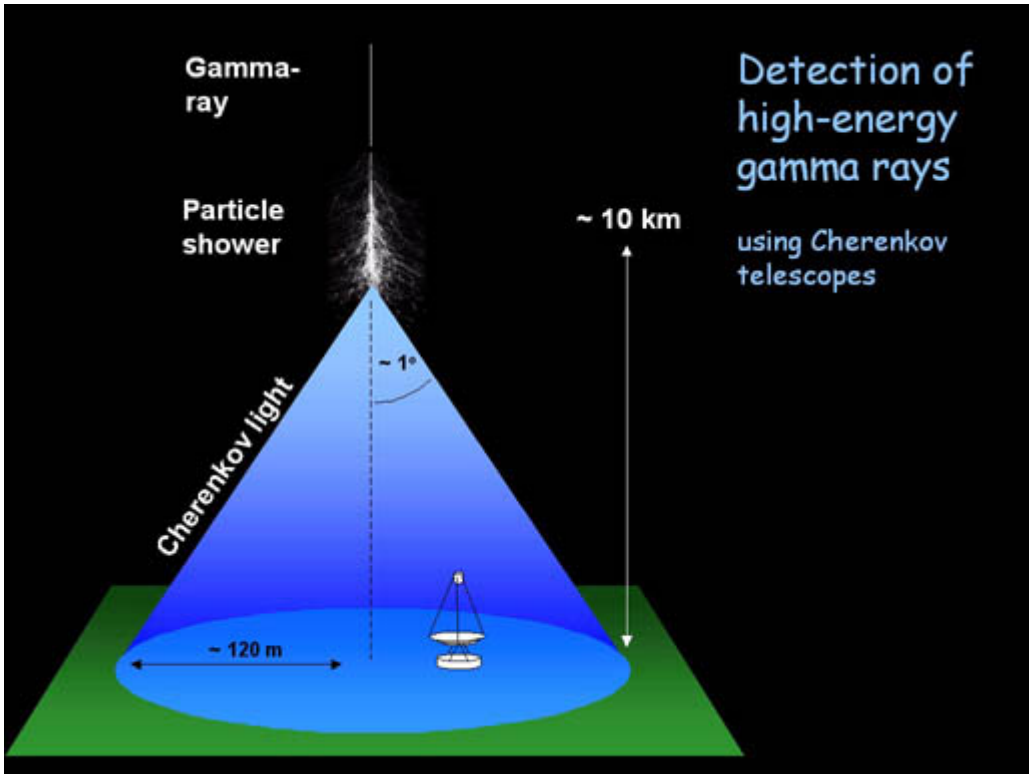

Figure 2.21: Detection of high energy gamma rays using the Cherenkov light produced by the electrons and positrons of the electromagnetic shower induced by the primary gamma ray entering the atmosphere.

collimated and are fully relativistic (the electron mass is 0.5 MeV while we are talking about primary photons having energies in excess of several GeV). Each of these electrons (positrons) emits Cherenkov light on a cone having a small

[2] The characteristic lengths that govern shower developments are the radiation and interaction lengths for electromagnetic and hadronic showers respectively, the former being smaller than the latter. However the separation between photon-induced and nucleus-induced showers is not an easy matter and must rely as well on the absence of muons in the photon case. It is a source of background.

aperture[3], of the order of 1°, with respect to its direction. This light illuminates an area on ground of the order of 5 10^4 m^2, called the Cherenkov light pool. It is collected by large mirrors, each seeing the whole shower but only part of the Cherenkov light, that which happens to have the right direction to be detected in the mirror (Figure 2.22). Several such mirrors sample the area, making it possible to reconstruct the shower axis, which is directed along the momentum of the incident photon, and to evaluate the shower energy, to something like 15%, from the dependence of the signal intensity on the distance of the mirror to the shower axis (the shower impact on ground is measured with an accuracy of about 30m). As shown in Figure 2.22, the Cherenkov light associated with cosmic muons

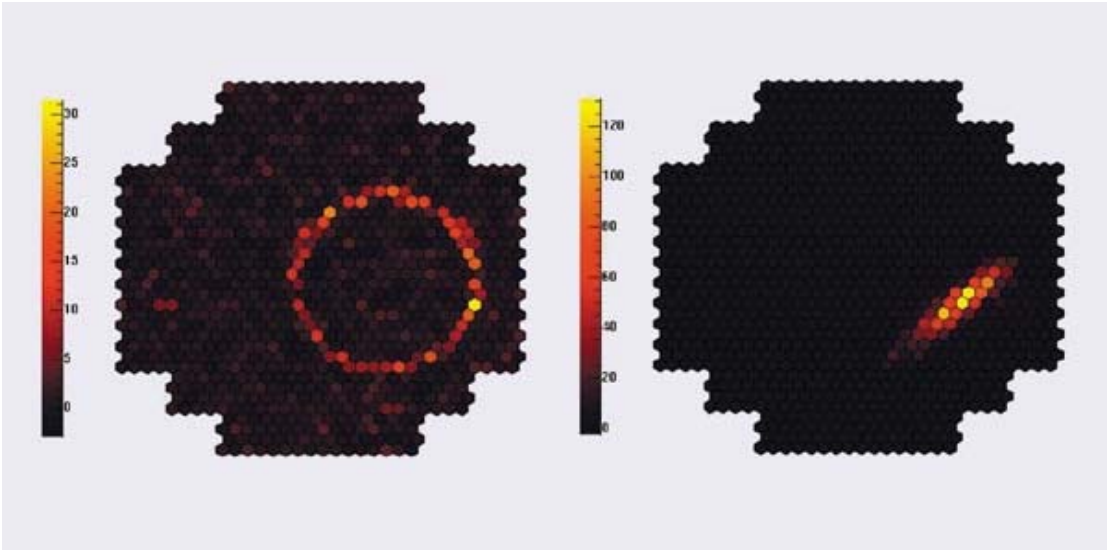

Figure 2.22. An image of a muon captured by the mirror of a Hess telescope (left) and a typical image of a shower (right).

hitting one of the mirrors generates a Cherenkov ring (because the muon radiates over a very long distance and keeps always the same direction). As the shower signal stays within a few nanoseconds (because of the short shower length), it is advantageous to use as fast as possible a detector in order to minimize the random background noise coming from the night sky and falling within the time window of the detector.

[3] At 10 km altitude, the pressure is about exp(-10/7.8)=0.28 atm. The index of refraction n of air at 1 atm is 1+2.9 10^{-4}, at 0.28 atm it is therefore 1+0.8 10^{-4}.
The Cherenkov angle θ is arcos(1/n), that is $1-0.5\ \theta^2 = 1 - 0.8\ 10^{-4}$, namely θ=.013 rad=0.7°.

The High Energy Stereoscopic System (HESS, located in Namibia, Figure 2.23 and 2.24), includes four telescopes at the corners of a 120×120 m^2 square and operates above the 100 GeV energy range. In each telescope, the Cherenkov light is collected by a mirror having an area of 108 m^2 and a reflectivity in excess of 80 percent. It is segmented into 382 smaller circular mirrors of 60 cm diameter each, made of quartz coated aluminized glass (Figure 2.25). Their orientations are individually adjusted to direct the light toward a camera located on the telescope axis. The telescope can only be operated during clear moonless nights.

Figure 2.23: One of the HESS telescopes

Figure 2.24. The HESS observatory in Namibia is a set of four Cherenkov telescopes.

The camera includes 960 photomultipliers arranged as a pixel array (Figure 2.26). The electronics samples and records the signals of the light detectors at 1 GHz. A trigger circuit is used to select good candidates that are recorded for further analysis.

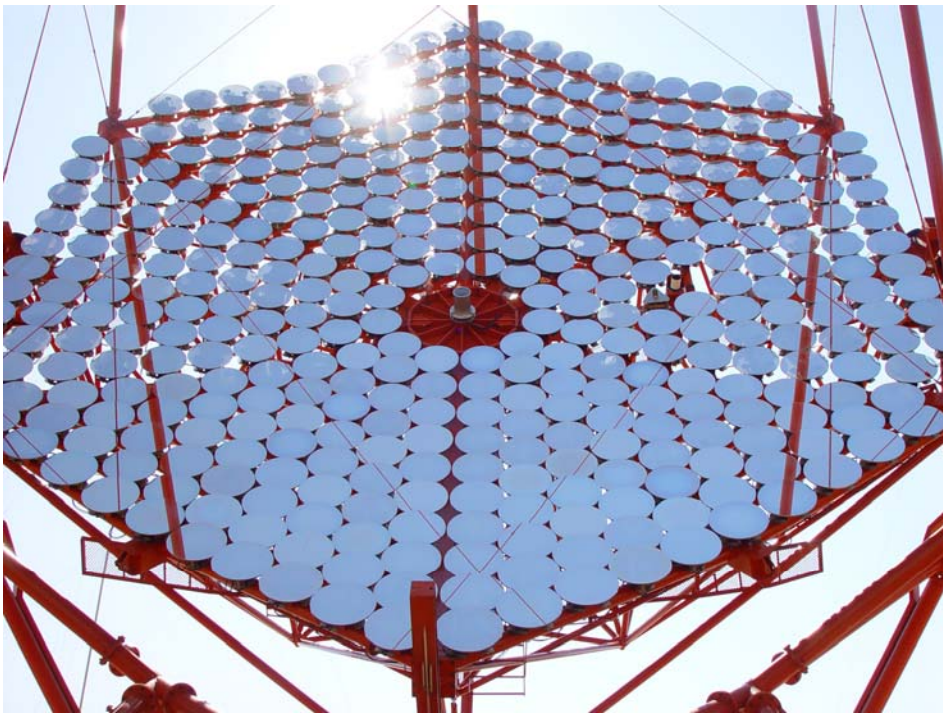

Figure 2.25. The mirror of each HESS telescope is made of 382 smaller orientable mirrors.

The field of view is 5^{o} and the resolution is a few arc minutes. Note that this is several thousand times worse than the best optical and radio resolutions: gamma ray astronomy is still a rather crude tool that does not allow for accurate association of the observed sources with their optical or radio counterparts. It is however progressing very rapidly: with HESS, it takes only 30 seconds to take a picture of the Crab while it was taking 50 hours a few years ago.

Gamma ray astronomy is good at detecting the high energy decay photons coming from neutral pions produced in the interaction of very high energy cosmic rays with interstellar matter (Figure 2.27). As gamma rays travel straight in the universe, contrary to cosmic rays that are bent in interstellar and intergalactic magnetic fields, they can be used to point back to the sources and to identify them.

HESS has been particularly active in the exploration of the galactic centre. We shall come back to these observations in Chapter V. Here we simply show in Figure 2.28 the first image of the region published by the collaboration. It shows a high gamma ray flux over the whole galactic plane dominated by two sources, the most intense of which has no identified counterpart. The other, fainter one is associated with a known super nova remnant (SNR).

Figure 2.26: The HESS camera in the process of being filled with photomultipliers.

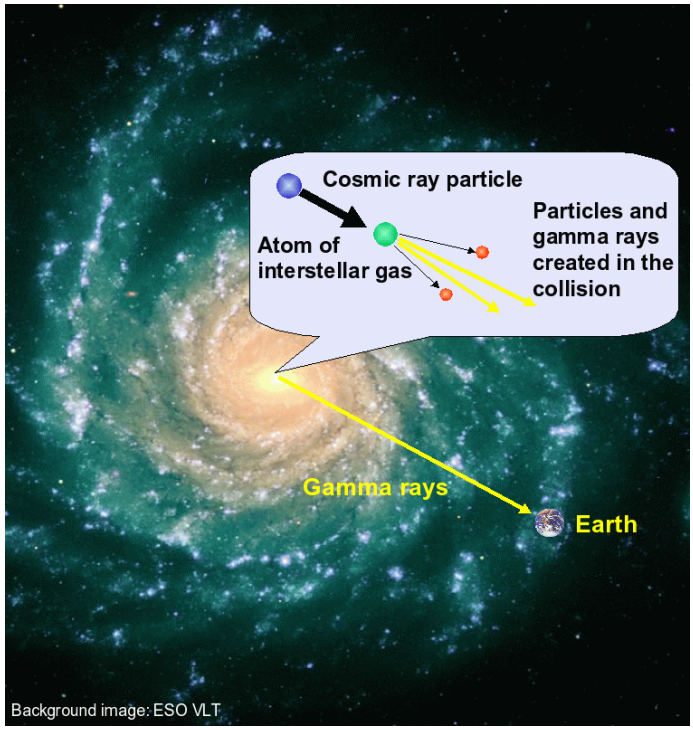

Figure 2.27. A cartoon illustrating the production of gamma rays from a cosmic ray interaction in the gas clouds

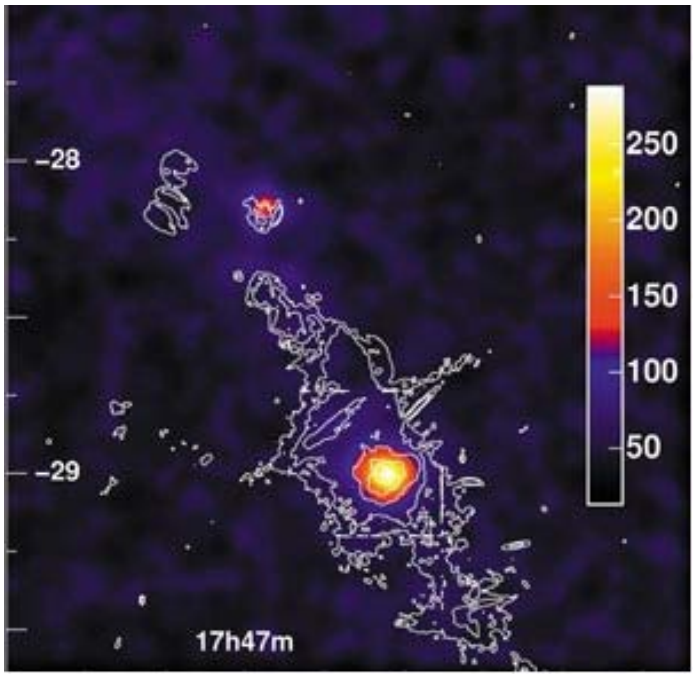

Figure 2.28. A HESS TeV image of the Galatic centre. The bright spot (HESS J1745-290) is in the SgrA region and corresponds to an unidentified source. The smaller spot corresponds to a supernova remnant (G0.9+0.1). The angular distance between the two is of the order of 1^{o}.

CHAPTER 3

THE RADIO SOURCE Sgr A*

The emission of radio waves from the centre of the Milky Way was first discovered in 1932 by Karl Jansky. At that time the resolution was not sufficient to resolve precisely what was the source. Indeed later observations have shown that there existed many radio sources in the region observed by Jansky. It was only in 1974 that Bruce Balick and Robert Brown resolved Sgr A* using the Green Bank radio telescope in West Virginia operated at 0.6 to 30 cm (Figure3.1) and noted that its emission varied by typically ± 10% on a scale of several to a few hundred days.

Figure 3.1: The 100 meter Green Bank Radio Telescope in West Viginira, USA.

The centre of the Milky Way is located in the Sagittarius constellation at a distance of some 25 000 light-years from us (Figure 3.2). At such a distance 1 arc min corresponds to 7.3 ly and 1 ly to 8 arc sec. Its declination and right ascension

are respectively δ=–28.9^o and α=266.4^o. That means that it can only be seen south of 61^o N latitude. In practice, to allow for observations of reasonable duration and to avoid important absorption in the atmosphere, good quality measurements of the galactic centre can only be done in the southern hemisphere or, in the northern hemisphere at tropical or lower latitudes. In particular, in Hanoi, at 21^o N latitude, the galactic centre is in our sky 39% of the time and reaches a maximum elevation of 40^o above the horizon. It is in the night sky in summer. We recall here that the angle between the Milky Way plane and the equator is 63^o.

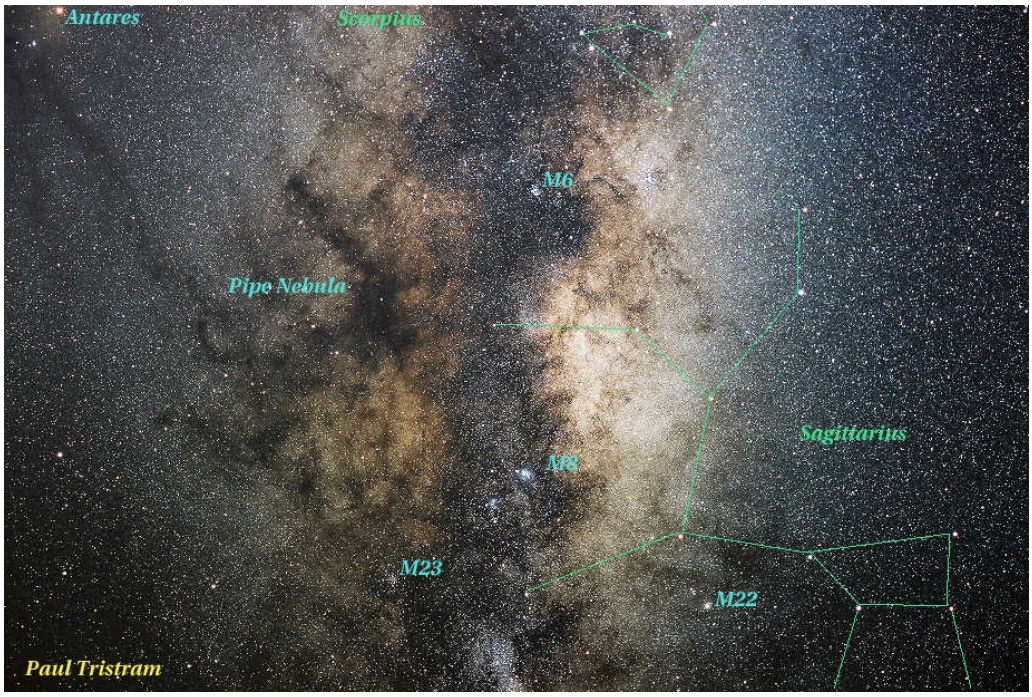

Figure 3.2: A view of the centre of the Milky Way, in the Sagittarius constellation, in the visible.

Figure 3.2 shows the region of the galactic centre as seen at visible wavelengths. As was said already, the centre itself is completely hidden by a thick veil of dust. In the radio range, however, the dust grains, which are typically micron size or less, do not obscure the view. But only sources emitting a large enough flux of radio waves can be seen, which is not the case, in particular, of normal stars. Radio views of the galactic centre are shown in Figures 3.3 to 3.5 at wave lengths of 90, 20 and 6 cm respectively. In practice most radio sources in this region reveal the presence of hot gas organized in different structures. The

presence of relatively high magnetic fields, up to 1mG or so, (remember that the galactic interstellar field is typically at the μG level) and of relativistic particles, in particular electrons, spiraling around the magnetic field lines, causes the emission of soft bremsstrahlung photons, a process called synchrotron radiation emission, which populate particularly the radio spectral range. Besides these non thermal sources there are also thermal sources associated with gases in thermal equilibrium. Among the radio sources in the galactic centre, it is convenient to consider separately the supernova remnants (SNR), various structures having the form of arcs or filaments and, finally, Sgr A* itself.

A general and essential feature of the galactic centre is that it is extremely crowded. As evaluated from observations in the infrared, the star density in its neighborhood is typically one million times larger than in the environment of the solar system. This is also apparent from the large number of SNR radio sources observed in the region. They can usually be identified from their shapes and from the properties of their eventual counterparts at other wavelengths. The high density of matter that accumulates in the galactic centre causes this region to be an active star forming region, like are OB associations, but with a higher rate of star formation. Moreover, higher mass, and therefore shorter lifetime, stars are being formed. As a result, the rate of supernovae explosions is particularly high.

The arcs and filaments have been, and still are, the subject of intense studies. Some of the filaments have been observed to have an X-ray counterpart that has been simultaneously studied. Their exact nature is not yet precisely known. Evidence that they contain high densities of hot ionized gas is obtained from the study of their spectrum. The filaments being often, but not always, directed perpendicularly to the galactic plane suggests a strong relation with the ambient magnetic field which is observed to reach as much as 1mG in some cases. The filaments are typically 10 to 100 ly long and 1 to 3 ly wide and occur within two degrees or so from Sgr A* exclusively. Recently, a multi-wave length study conducted at Green Bank (Figure 3.6) showed that some filaments having a non-thermal emission are connected with star forming regions (thermal emission) formerly identified using the VLA and containing each some hundred massive stars. It seems that strong stellar winds occurring in the region play an important role in their formation.

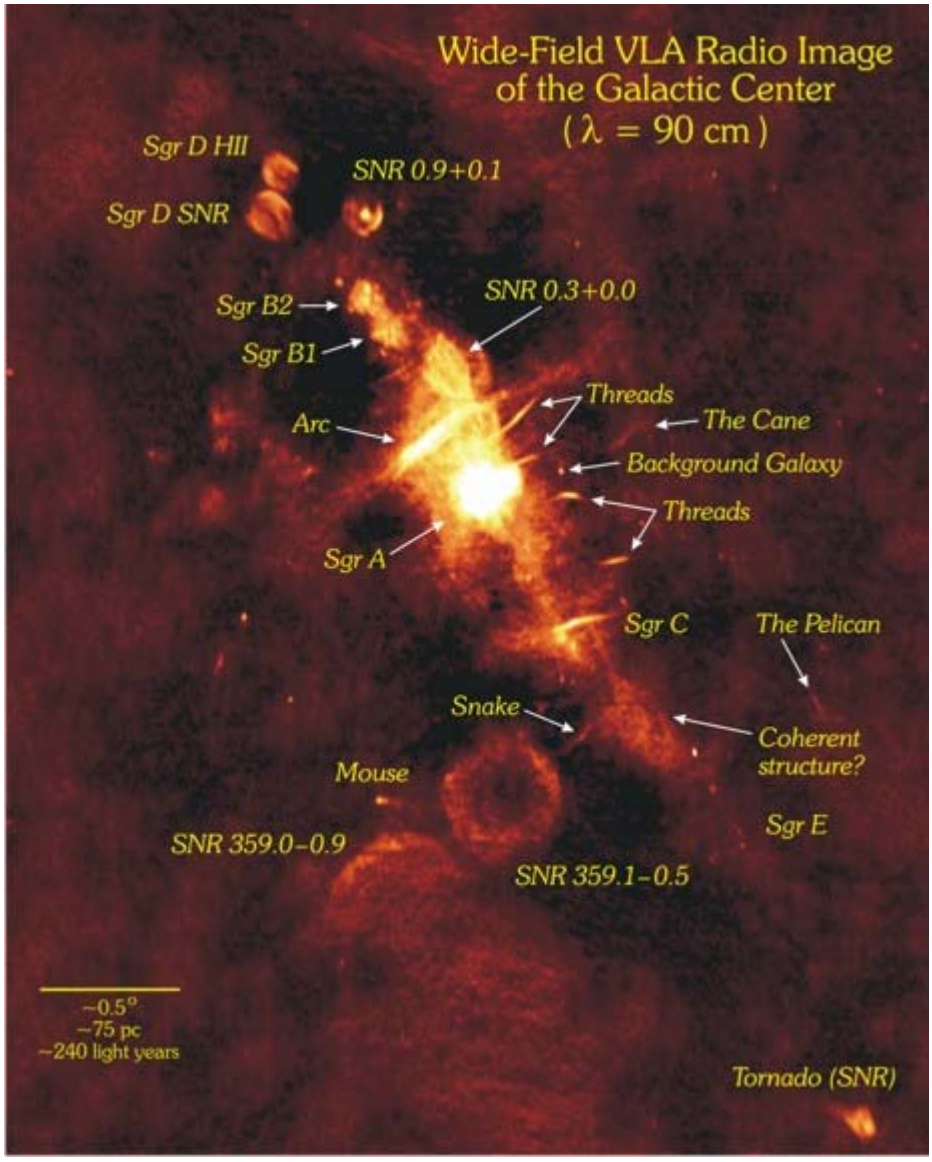

Figure 3.3: The 90 cm radio image of the Galactic centre showing some SNR's, radio arcs, filaments, and the Sgr A* region.

With higher and higher resolutions, radio astronomers have succeeded to zoom closely to the galactic centre (Figures 3.7 and 3.8). While the eastern part of Sgr A is thought to be a SNR, the western part is associated with hot gases spiraling down to the black hole. It is important at this stage to keep a few scales in mind: the Schwarzschild radius of the sun being 3 km , that of a black hole having a mass of 3.6 million suns is 10.8 10^6 km, (36 ls or 1.2 10^{-6} ly). The field of view of the VLA image of Figure 3.8, showing Sgr A* as a bright dot in its centre, has a

field of view of approximately 2 ly × 2 ly. The field of view of the infrared NAOS image shown in Figure 4.4 is of the order of 0.12 ly × 0.12 ly. The best limits on the Sgr A* diameter are of the order of 1 AU, that is 1.6 10^{-5} ly.

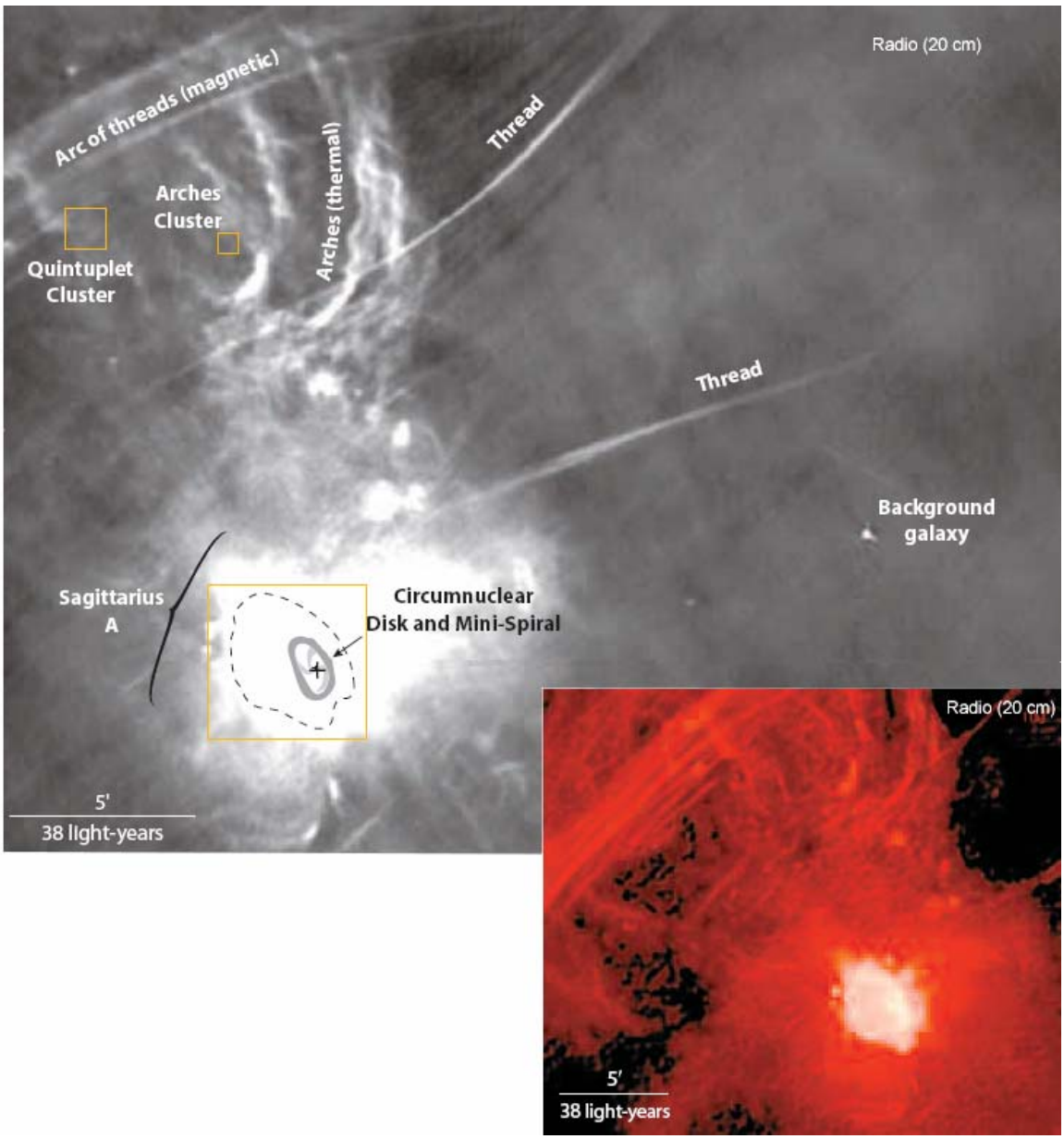

Figure 3.4: These 20 cm radio images show some features of the Galactic centre: turbulent arcs, magnetic threads, and the powerful Sgr A radio source. The insert shows an enlarged view of the Sgr A region.

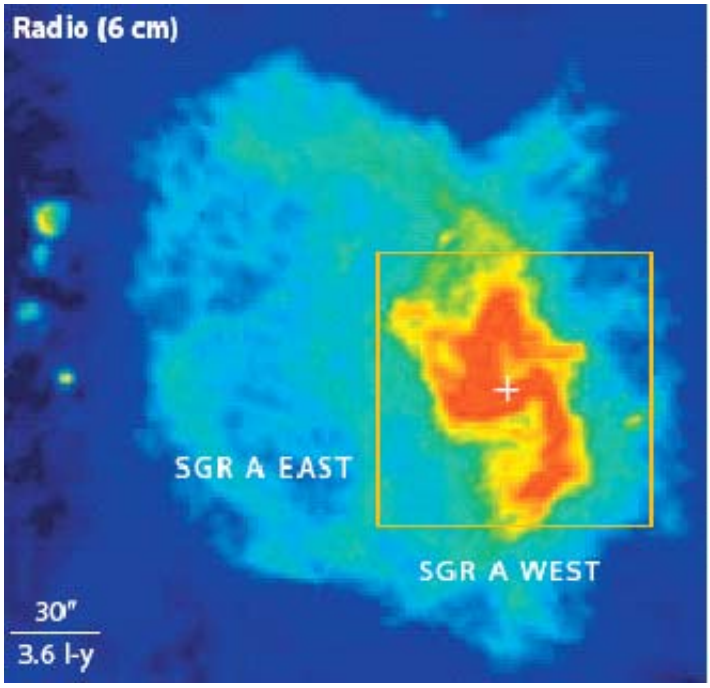

Figure 3.5: A 6 cm radio image of the Sgr A region. It shows the SNR Sgr A East on the left. On the right, SGR A West is centered on Sgr A*. An enlarged view of the insert is shown in Figure 3.7

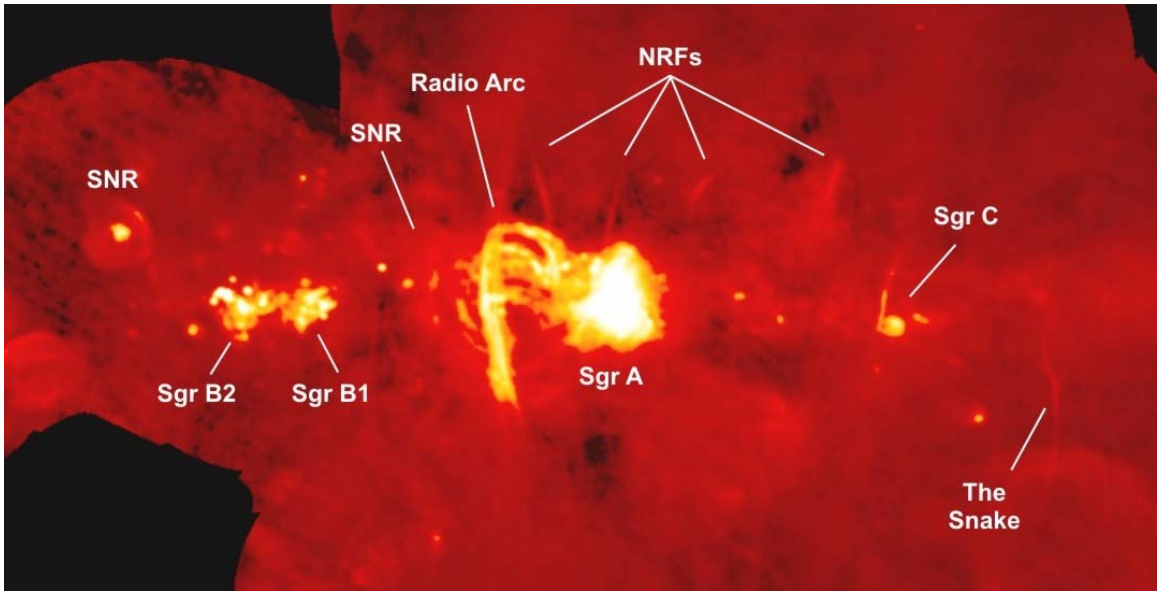

Figure 3.6: The region surrounding Sgr A shows some non-thermal radio filaments (NRFs) besides SNR's and other features. The image was obtained by combining data from the VLA and multi wave lengths exposures from the GBT.

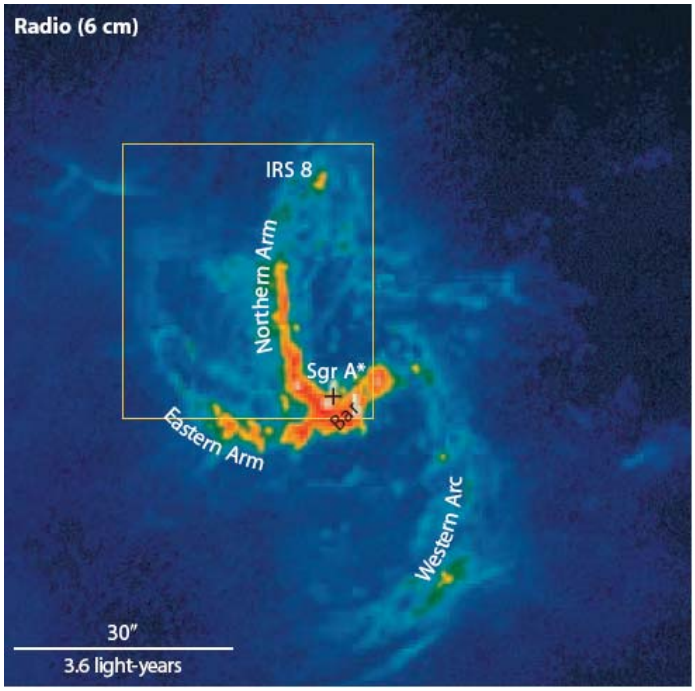

Figure 3.7: A high resolution image of Sgr A showing the three spiral arms of the Mini-spiral.

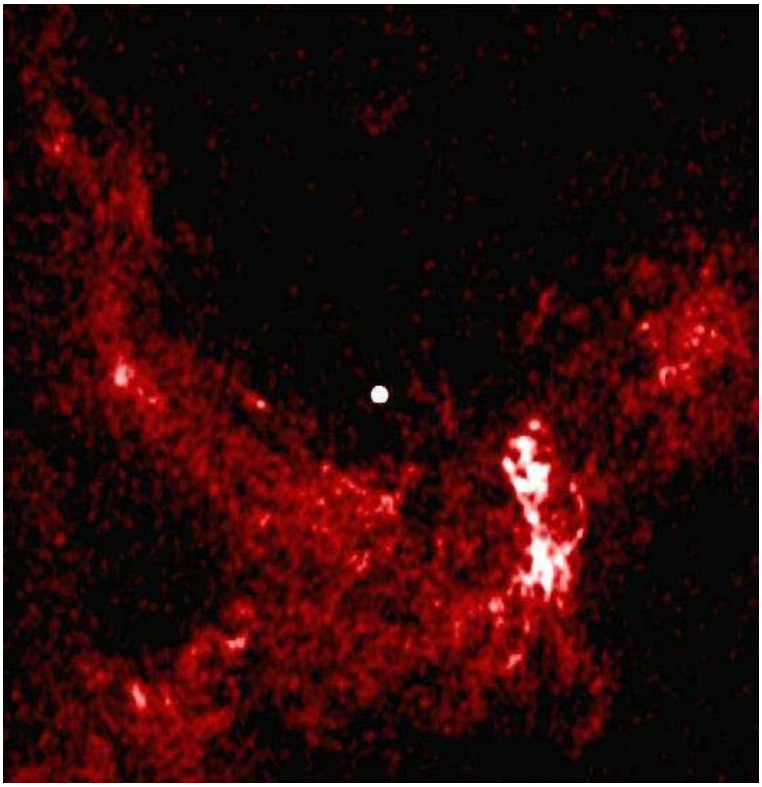

Figure 3.8 The closest VLA image of the galactic centre showing Sgr A* as a bright spot in the middle of the field

The black hole is surrounded by a ring (or disk) of dust and gas, the circum-nuclear-ring (Fig 3.9), orbiting SgrA* at a mean radius of about 6.5 ly and at a velocity of 110 km/s. Ammonia emission at 1.3cm wavelength has been studied with the VLA (allowing for a resolution of 0.13 ly) in the region of the circum-nuclear ring. It shows streamers coming from very dense clouds located at 25 to 50 ly from SgrA* and feeding the circum-nuclear-ring, probably attracted by the strong gravitational pull of the black hole as their velocities are measured to increase when approaching the centre. Using VLA observations made over ten years, Yusef-Zadeh has shown that the spiral arms visible on Figures 3.7 and 3.8 are made of hot (more than 10 000 degrees) ionized gas whirling around the black hole.

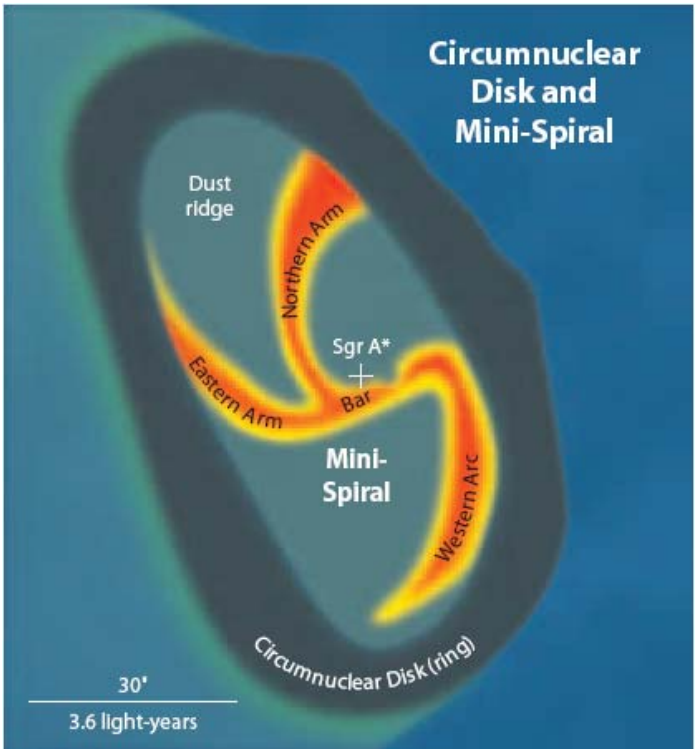

Figure 3.9: A schematic drawing of the innermost few light years around Sgr A*.

Recent measurements using the Very Long Baseline Array (VLBA) brought new detailed information on Sgr A*. The VLBA is an array of ten 25 m diameter radio telescopes spread over the northern hemisphere from Hawaii to the Virgin Islands (Figure 3.10). All telescopes can operate between 90 cm and 7 mm wavelengths. Measurements carried over two years have been able to detect the

movement of Sgr A* shifting by several diameters each year. Most of it is due to the movement of the sun orbiting the Galaxy. Once this apparent movement is subtracted, the proper velocity of Sgr A* is shown to be less than 20 km/s, a very low value consistent with the idea that Sgr A* is a very massive black hole anchoring the centre of the Milky Way. More recent VLBA observations at two different wavelengths have allowed to place a limit on the diameter of Sgr A* of less than 10^{-5} ly.

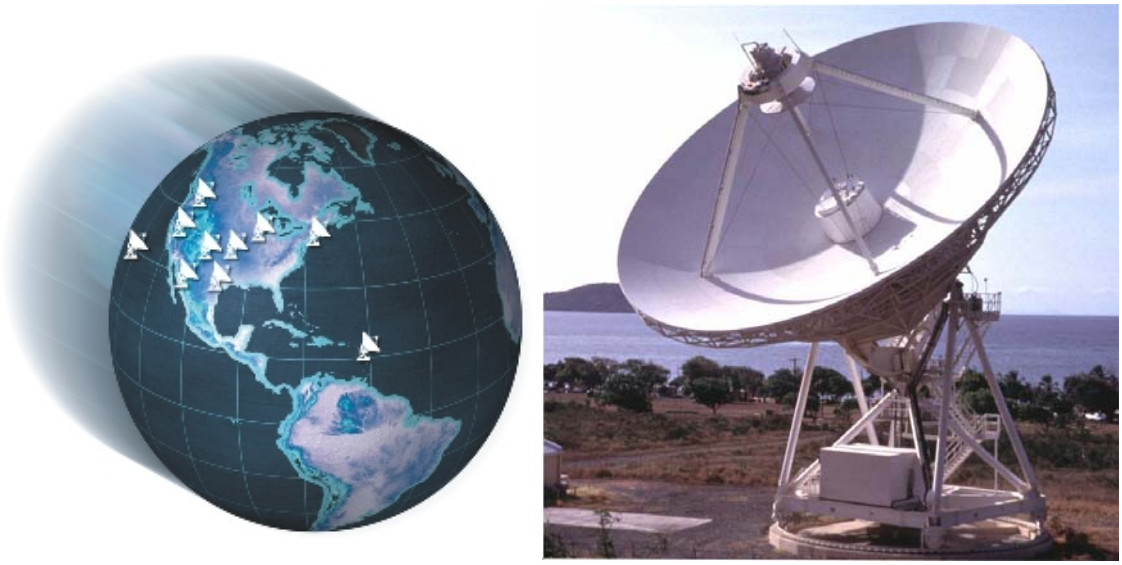

Figure 3.10: The Very Long Baseline Array (VLBA) includes ten 25 m radio telescopes spread over the northern hemisphere. The photograph shows one of them in Hawaii.

Note that at shorter wavelengths, in the microwave regime, observation can only be made from space or at very high altitudes. Figure 3.11 shows a view of the galactic centre region taken with the Cosmic Microwave Background Explorer (COBE) that made the first high precision measurement of the CMB map and spectrum. It shows emission from the gas and dust in the galactic plane at microwave frequencies.

In summary, the progress achieved during the past thirty years has allowed radio astronomers to accumulate an impressive amount of information on the Sgr A region, all supporting the presence of a massive black hole in its centre. The surroundings are seen as a very crowded star formation region containing a large

number of SNR's and hot plasma structures, arcs and filaments, which are the seat of large magnetic fields. At the centre, Sgr A* is seen as a very bright spot toward which three spiral arms of hot gas are whirling, themselves coming from a ring or disk of dust, of radius 6.5 ly, fed from large clouds at distances of 25 to 50 ly. Of course, it is not the black hole itself that is being seen but hot matter somehow falling into it. Whether the radio emission comes from an accretion disk, or polar jets, or something else will be the subject of future studies. New projects, such as the Alacama Large Millimeter Array (ALMA), are already preparing for it.

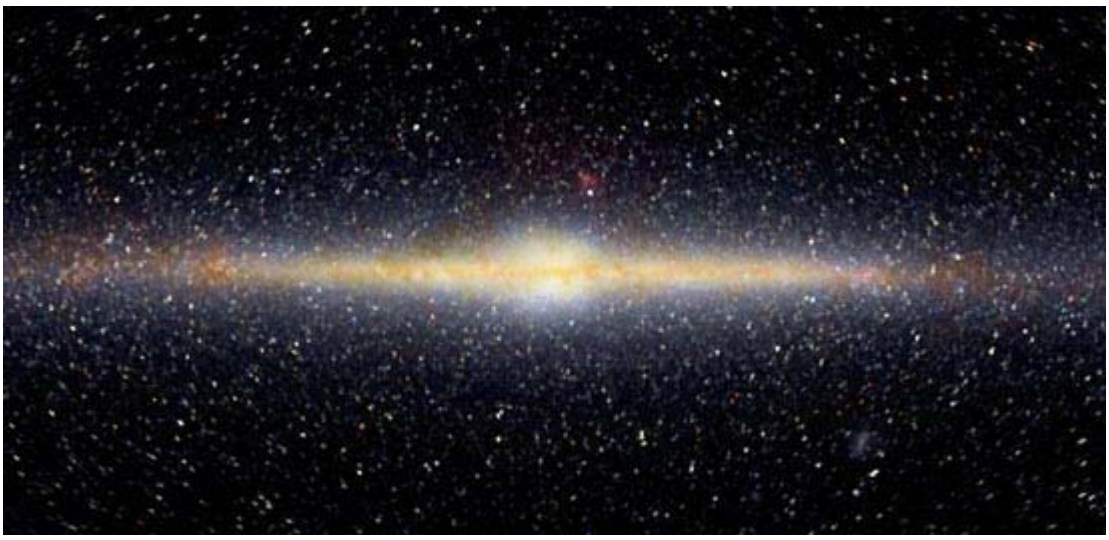

Figure 3.11 COBE image of the galactic centre.

CHAPTER 4

STARS ORBITING AROUND SGR A*

While the galactic centre is completely obscured at visible wave lengths (an optical extinction of 30 magnitudes!), one can start seeing it glowing in the near infrared (Figure 4.1). The fraction of light transmitted at 550 nm is only one billionth; at 2200 nm it reaches 10%. At larger wave lengths the most brilliant stars are therefore visible (Figures 4.2 and 4.3). The observations that have been made of the movement of such stars are one of the richest sources of information available on Sgr A*. Two such stars, S2 and OS16, have been carefully studied by a European and an American group respectively. We shall now concentrate on the first of the two that was observed using the VLT equipped with adaptive optics(NAOS/CONICA) as was described earlier on.

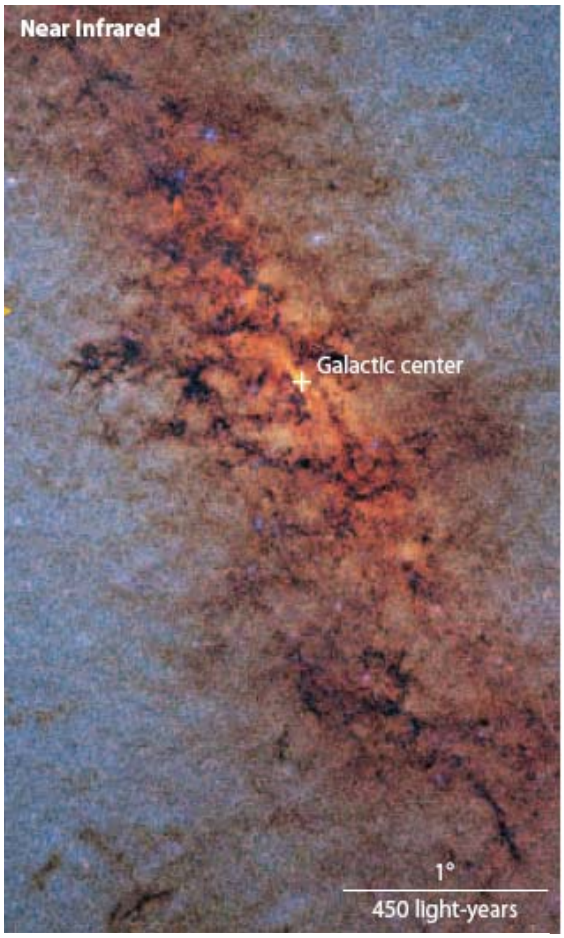

Figure 4.1 A near IR view of the galactic centre (in false colors, infrared wavelengths are divided by 3).

Early measurements using the VLT and NAOS' predecessor (called Adonis) had already revealed the presence of very high velocity stars in the neighborhood of Sgr A*. In 2002, new observations were made by pointing the infrared wave front sensor of NAOS on a bright infrared star located only 6 arc sec north of Sgr A*. Luckily enough, it then happened that one of the monitored stars, called S2 (having an orbital period of 15 years), passed at its closest distance to Sgr A* during the period of observation. This distance was particularly small: 17

light hours, only three times the orbit of Pluto around the Sun (but still a factor 1700 above the Schwarzschild radius of Sgr A*).

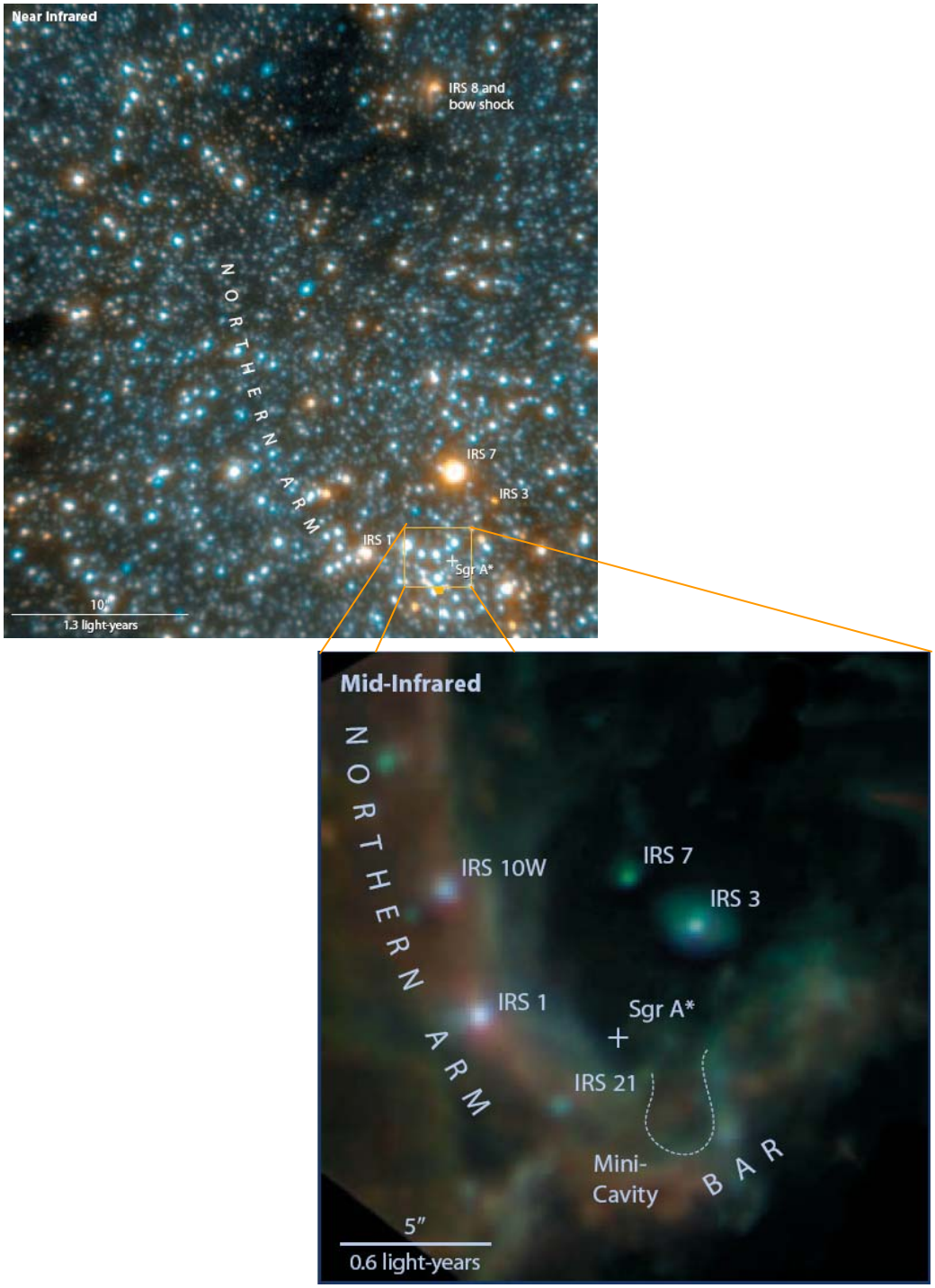

Figure 4.2 Mid IR view of the galactic centre, the enlarged image on the right covers the square shown on the top. Sgr A* is not visible on these images.

Figure 4.3. A composite IR image of the galactic centre taken at three different wave lengths (1.7, 2.2, and 3.8 μm). The square corresponds to the view of Figure 4.4.

Figure 4.4 shows the orbits of the stars observed, while Figure 4.5 shows the orbit of S2 alone[4]. The ellipses are fits to the observed positions. As the movement of a gravitationally bound body probes the value of the mass contained within the orbit, Kepler's laws allow placing a limit on it. This is illustrated on Figure 4.6 where the value of the enclosed mass is plotted as a function of radial distance to Sgr A*. As expected, the close passage of S2 near Sgr A* in 2002 severely constrains the value of the mass of the black hole to something like 3 to 4 million solar masses. The line in Figure 4.4 assumes a local star density (excluding the black hole) of 3.9 10^6 solar masses per cubic parsec; it gives a good fit to the data and corresponds to a black hole mass of 2.6 million solar masses. At the same time an upper limit of some 17 light hours on the Schwarzschild radius of the black hole is obtained from the fact that all orbits are elliptic, in particular that the orbit of S2 remains elliptic at its closest distance of approach.

[4] An animated view of these data is available on http:/www.mpe.mpg.de/ir/GC/index.php.

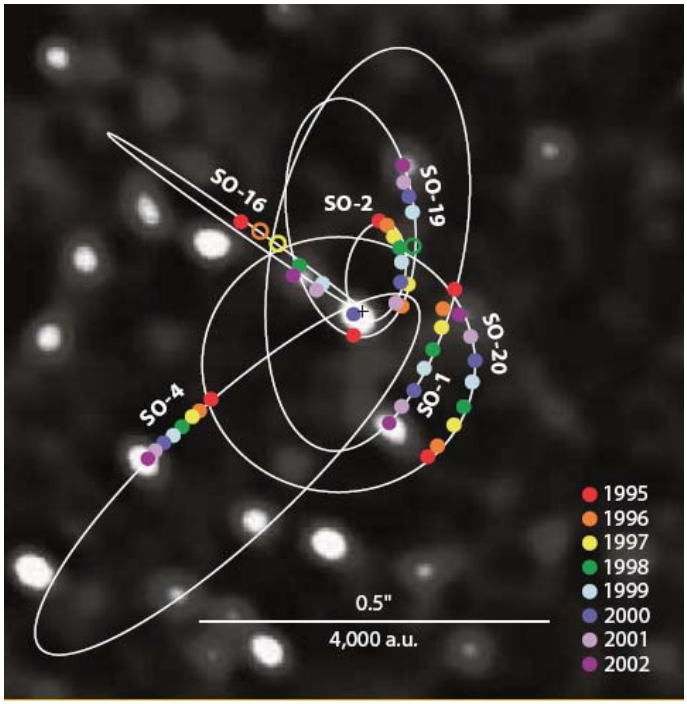

Figure 4.4 Infrared view of stars orbiting Sgr A* showing their elliptic trajectories and their positions between 1995 and 2002.

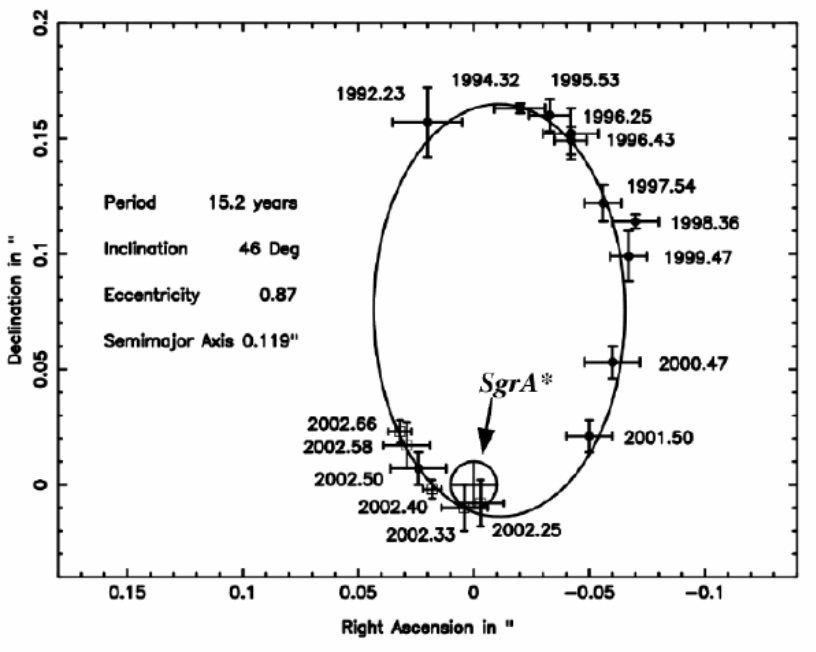

Figure 4.5 The orbit of S2 around Sgr A* as observed with the VLT (Adonis and NAOS/CONICA) between 1992 and 2002

A second and very important result obtained by the same group from ongoing VLT/NAOS/CONICA measurements, is the observation of a faint IR image at the precise location of Sgr A* (the radio source). This is illustrated in Figure 4.7. In fact what happened is that on May 9th 2003 a flare was observed at the position of Sgr A* at both 3.6 and 4.8 μm wave length. Looking back to the earlier data, a faint image could indeed be identified at the same position. More flares were subsequently observed in the H, K and L bands (respectively 1.7, 2.2 and 3.8 microns). They are consistent with the hypothesis that the IR emission is caused by the synchrotron radiation of relativistic electrons in the polar jets of plasma likely to be associated with the black hole. They would be associated with irregularities of the amount of matter being accreted and/or swallowed by the black hole. Their rise and fall time imply that the source is within less than 10 Schwarzschild radii from the black hole. The IR flares seem to show a modulation with a 17 mn period. If it were to correspond to the last stable orbit of the black hole it would imply a very high spin, about half of the maximum possible for a Kerr black hole.

The results obtained by the American group used the 10-meter Keck 1

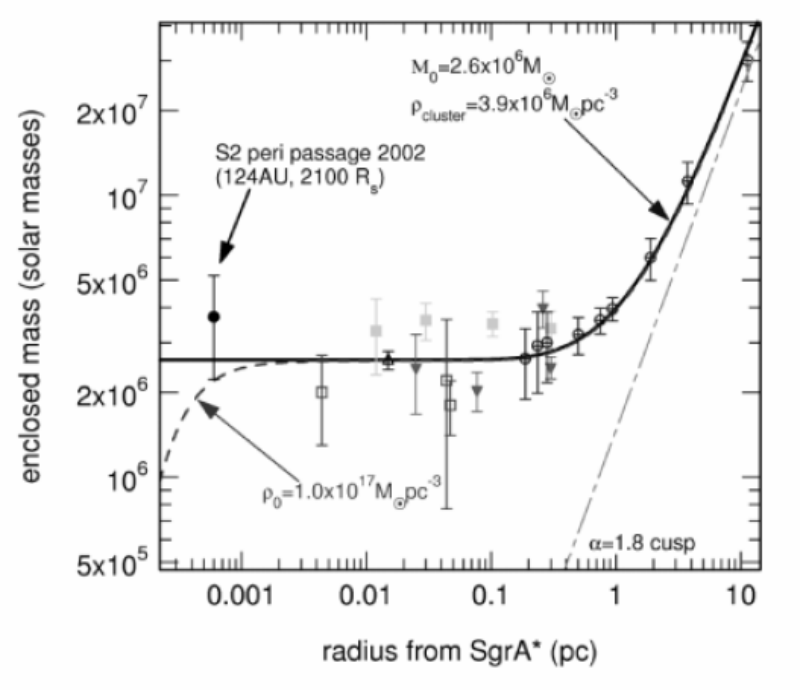

Figure 4.6 Dependence on the distance to Sgr A* of the mass enclosed within the star orbits.

infrared telescope atop Mauna Kea in Hawaii, with infrared speckle interferometry replacing the adaptive optics. They also observed some flares.

Infrared images of the galactic centre not only tell us about Sgr A* but also about its very dense environment. In its immediate surroundings, in the region of the Mini-spiral, several interesting objects are to be seen. They include a collection of hot and windy stars; a small bubble, called the Mini-cavity, which was blown by one or more hot stars; a type M super giant, IRS7. Millions of stars of various masses and spectral types crowd the field around the core of the central star cluster (IRS16), including M giants and super giants as well as hot, massive O and B stars (Figures 4.2 and 4.3). The simultaneous presence of young blue super giants and older red giants indicates multiple epochs of star formation as expected from sporadic cloud collisions. The strong gravitational field of Sgr A*, together with turbulent stellar winds and important magnetic fields, make it more difficult for light clouds to collapse than in a more quiet environment: as a result higher mass stars are formed than elsewhere in the Galaxy. Some of the brightest stars, including ISR8, have diffuse nebulae surrounding them, witnessing important winds that form shock fronts when meeting dust clouds.

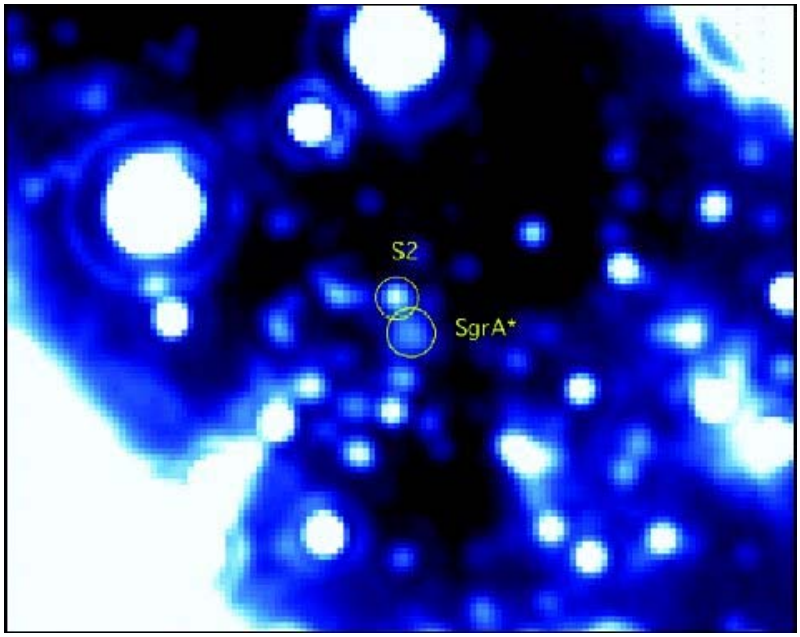

Figure 4.7 A close-up IR view of the galactic centre showing the faint emission from Sgr A* (at 3.6 and 4.8 μm) and the neighbor S2 star.

CHAPTER 5

FLARES, X-BINARIES, AND TEV PHOTONS

It was not until the new century that the X-ray counterpart of Sgr A* could be identified. In January 2000, Baganoff et al. reported its first observation using the CHANDRA X-Ray satellite, which has been described earlier, together with ACIS, the Advanced CCD Imaging Spectrometer (Figure 5.1), a high resolution device. The resolution of earlier observations was not sufficient to detect the relatively faint source. Figures 5.2 to 5.4 show a series of X-ray images zooming toward Sgr A*. The 2 to 8 keV X-ray image superimposed on a mid-IR image in Figure 5.4 shows the unambiguous identification of the source. It has now been possible to give evidence for the fact that Sgr A* is an extended X-ray source with an intrinsic size of emission of 1.4 arc sec (full width at half maximum) consistent with what is expected from the accretion disk of a black hole having a mass of 3 millions solar masses.

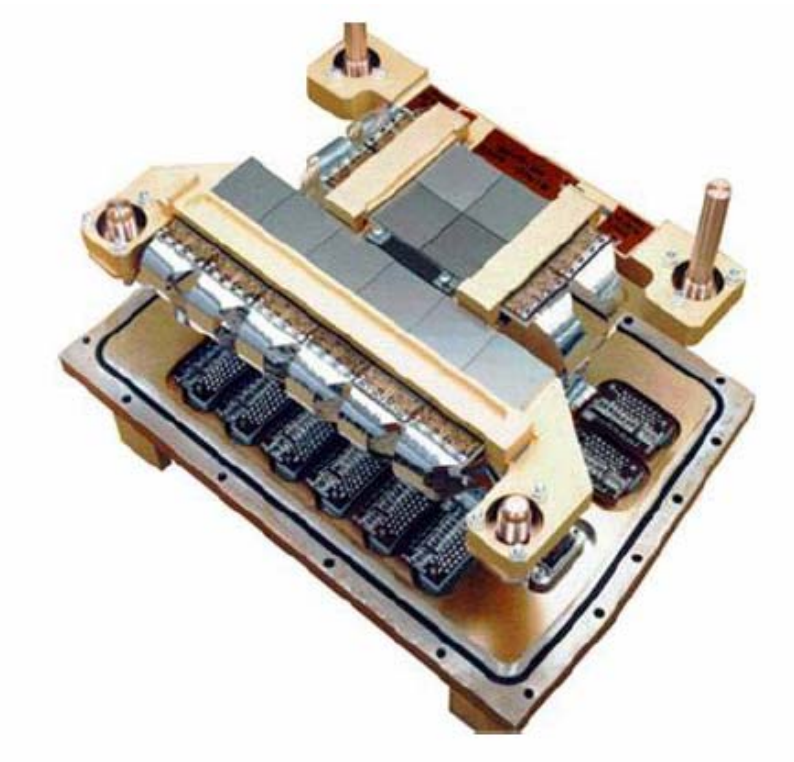

Figure 5.1: The CHANDRA Advanced CCD Imaging Spectrometer (ACIS).

Figure 5.2. X-ray view of the galactic centre as seen by CHANDRA (2×0.8^{o}).

Figure 5.3. Close up of Figure 5.2

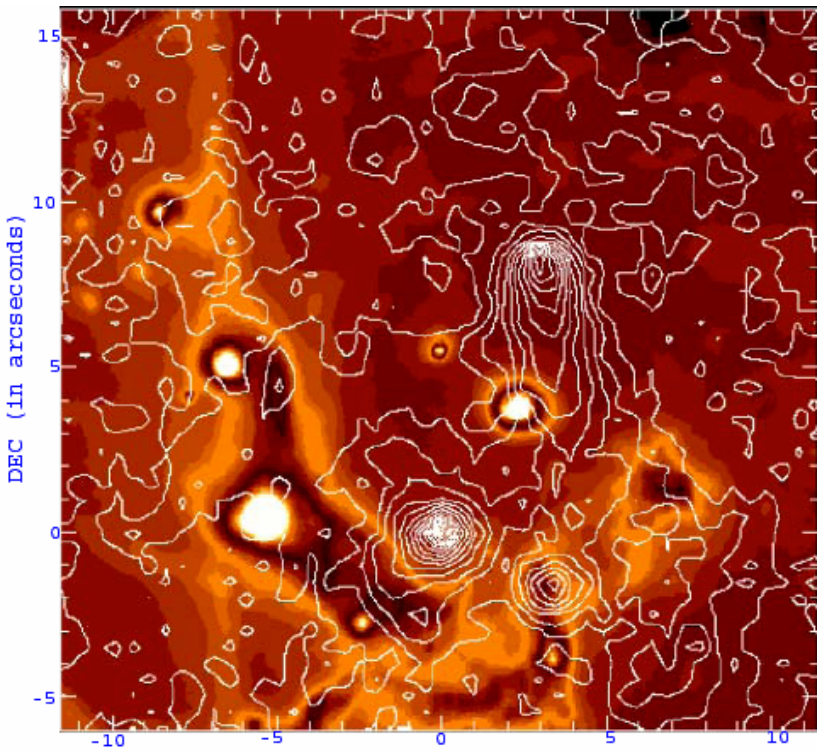

Figure 5.4. Close-up on the galactic centre: 2-8 keV X-ray contours from CHANDRA are superimposed onto the false color image of NAOS/CONICA at mid-IR. Sgr A* is at the origin of coordinates.

A remarkable feature of the X-ray data is the observation of occasional flares of short duration, typically one hour. Flares standing at least ten times above background occur about once every other day. The emission may rise by as much as a factor of 100 during several 10 minutes. Figure 5.5 shows a particularly striking occurrence of three strong flares within a bit more than a day. The observation of such flares in simultaneity with IR flares detected by NAOS/CONICA has recently been reported. A remarkable feature is that Sgr A* is the only X-ray source, among the 2300 X-ray point sources present in the field of Figure 5.3, to show this flaring behavior. The short duration of the flares implies the compactness of the source, providing another strong argument in favor of the identification of Sgr A* as a black hole. X-ray emission of the kind that is detected is expected from the synchrotron radiation of electrons spiraling along the polar jets directed along the angular momentum of a spinning black hole (so-called Kerr black hole), perpendicularly to the accretion disk at the equator. As in the IR case, the flares would then correspond to irregularities in the amount of matter being attracted to the accretion disk and/or from the disk to the black hole. While Sgr A*

emits X-rays in its quiescent state from a slightly extended region around the black hole, giving probably evidence for hot accreting gas, during X-ray flaring a distinctive point source becomes visible at the location of Sgr A*.

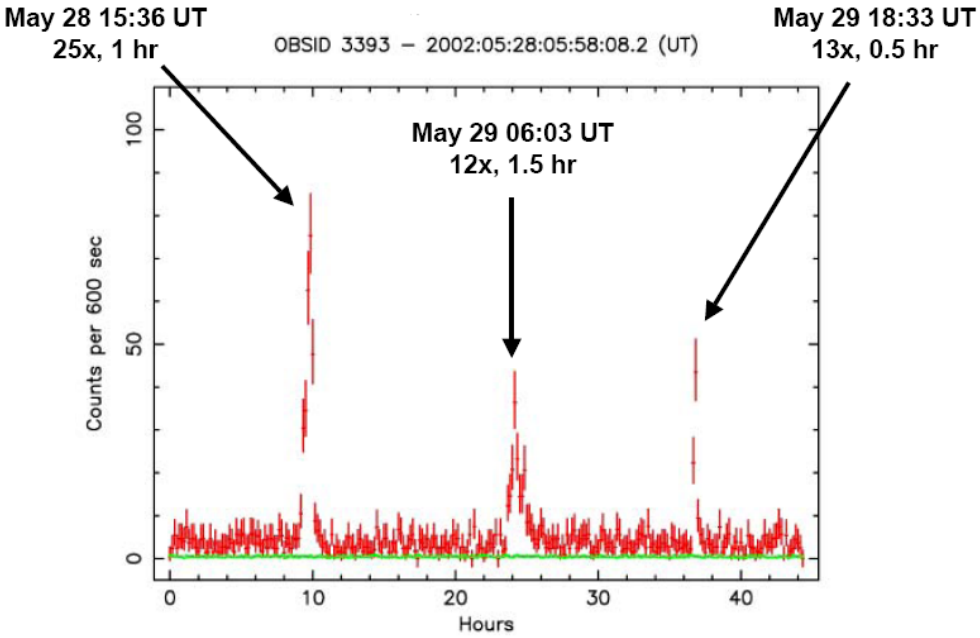

Figure 5.5. Three X-ray flares observed in May 2002.

The recent likely observation of a jet-like structure at right angle to the galactic plane, namely parallel with the direction of the magnetic field, itself parallel to the axis of rotation of the black hole, has been reported (Figure 5.6). If confirmed it would be a very important discovery. X-ray images of the galactic centre show a very high density of X-ray sources in the environment of Sgr A*. In the field of Figure 5.3, 2287 X-ray point sources have been resolved. Figure 5.7 shows a close-up view of the galactic centre with five variable X-ray sources identified as active X-ray binaries, namely X-ray binaries of which one of the members is a black hole or neutron star accreting matter from its partner. Four of these (A, B, C and D) are located at less than three light years from Sgr A*, while only 0.2 would have been expected from the local density of stars. This factor 20 enhancement suggests that a large number of stellar black holes, having concentrated in the region of the galactic centre, collide with normal binary stars and exchange partner in the collision, leaving an active X-ray binary and a bachelor normal star. The presence of a high density of stellar black holes near the

galactic centre is consistent with the idea that stellar black holes, when colliding with lighter stars, tend to loose energy on average and therefore drift toward the galactic centre. If this explanation is true, a swarm of some 10 000 stellar black holes may be orbiting Sgr A*.

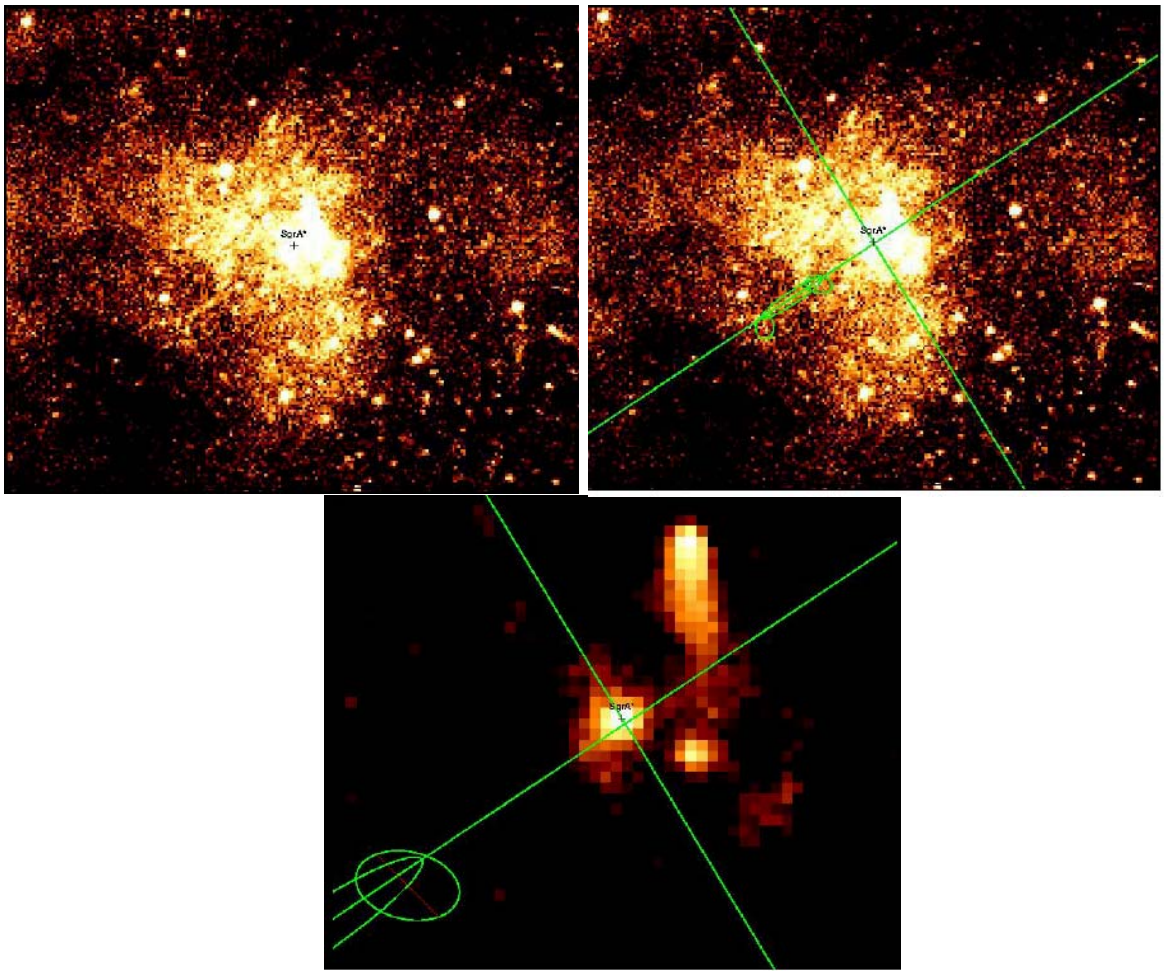

Figure 5.6. X-ray view of the SgrA* region showing a possible jet (upper-left) glowing in the region indicated on the upper-right, perpendicularly to the galactic plane. A close-up is shown in the lower part.

Figure 5.8 shows additional X-ray views of the Sgr A* region. We may also mention at this stage that X-ray images of the galactic centre have allowed for the identification of X-ray filaments being the counterparts of radio filaments, both non-thermal. Their joint study has made it possible to evaluate the magnetic field in the filaments, of the order of 0.1 mG.

At higher energies, HESS has started observations of the galactic centre region. While unable to compete with the lower energy observations in terms of resolution, it has already produced a map of the galactic centre region in the TeV energy range (Figure 5.9). While some sources can be identified with known SNR's or AGN's, some others seem to have no counterpart in any of the radio, IR or X-ray range. If this were confirmed, it would be very puzzling, TeV gamma rays being usually considered as secondary products of cosmic ray interactions in the vicinity of the cosmic accelerator.

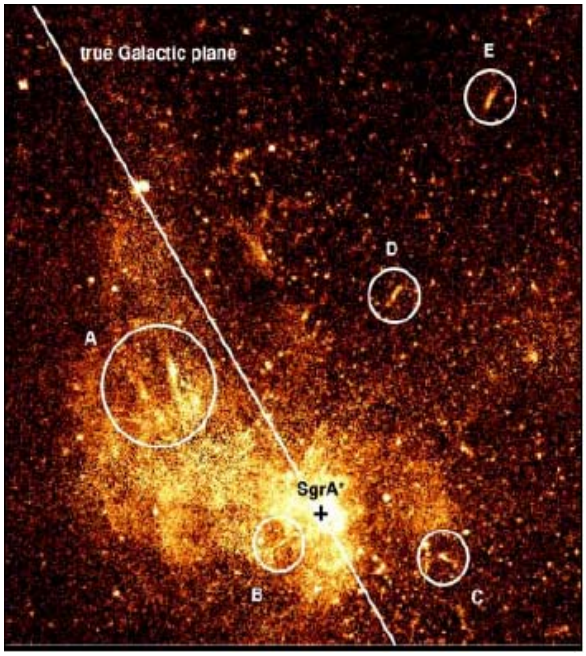

Figure 5.7. X-ray view of the Sgr A region with five X-ray binaries indicated by circles

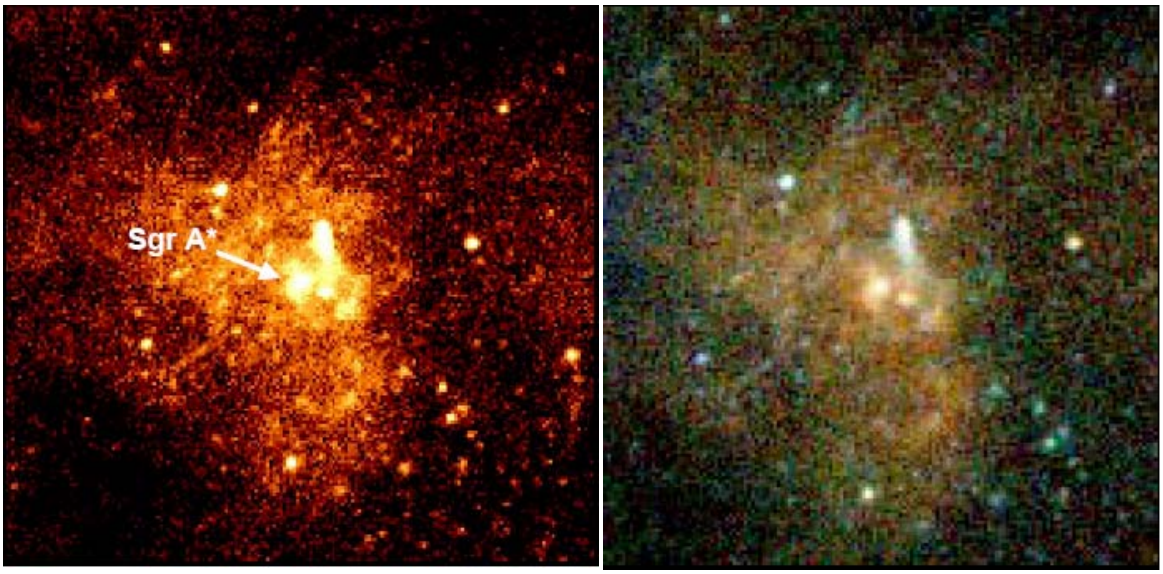

Figure 5.8. X-ray views of Sgr A West and Sgr A*. The figure on the right is a three color image.

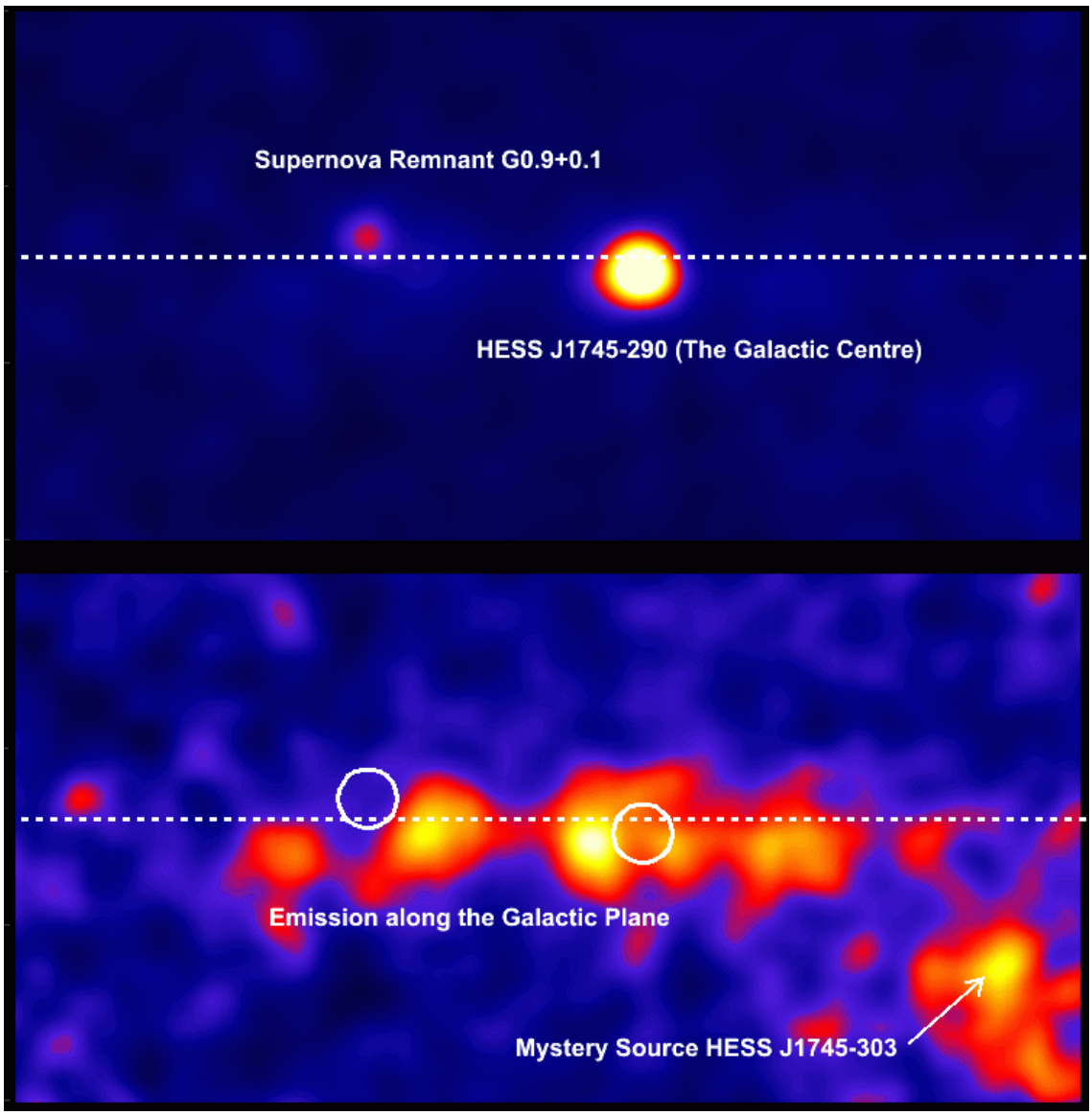

Figure 5.9: A 4^{o} wide view of the galactic centre region as seen by HESS. The top panel shows two bright sources dominating the view: HESS J1745-290, right at the centre of the Galaxy; and, about 1^{o} away, the SNR G 0.9+0.1. The lower panel shows the same image with the bright sources subtracted. In this image gamma-ray emission extending along the plane shows a source that seems to have no counterpart: HESS J1745-303. The dashed lines show the position of the Galactic Plane. The white circles show the positions from which the two sources were removed.

CONCLUSION

We end here our journey in the region of the galactic centre.

An amazing quantity of new results, most of them less than ten years old, have been presented, testifying the extreme vitality of this field of research. While there is no doubt any longer that a super-massive black hole, with a mass of three to four million solar masses, resides in the centre of the Milky Way, many results require confirmation and a host of future studies will be required before we may obtain a reliable description of the mechanisms at play. Our emphasis has been to show the beauty and richness of the data obtained and to present a summary of the arguments in favor of the currently accepted interpretation. However all these results must be critically examined and carefully ascertained.

In addition to telling us about the centre of our own galaxy, these results suggest that any galaxy is likely to have such a super massive black hole in its centre. At least, it has always been a good working hypothesis in astronomy and astrophysics to accept that there is nothing special about the place we live in...

Moreover, it seems now likely that we have at hand a model of the much more massive black holes that power active galactic nuclei (AGN) and quasars. There is no doubt that major progress is still to be expected in our understanding of Sgr A*. This will undoubtedly help our understanding of AGN's and quasars, whether by finding similarities or differences with the small scale model that we have at home.

The study of the galactic centre is in rapid expansion and will no doubt remain one of the central topics of interest in astrophysics for many years to come.

Bibliography

Most of the information used in making this review was obtained from the various web sites of the facilities or institutions working on the galactic centre:

They include, among others:

CHANDRA

Cosmic Observatory Background Explorer (COBE)

European Southern Observatory (ESO)

European Space Agency (ESA)

Green Bank telescope (GBT)

Harvard-Smithsonian Centre for Astrophysics

High Energy Stereoscopic System (HESS)

Hubble Space Telescope (HST)

Keck telescope

Massachusetts Institute of Technology (MIT) Centre for Space Research

Max Planck Institute für Extraterrestrische Physik, Garching

National Aeronautics and Space Agency (NASA)

National Radio Astronomy Observatory (NRAO)

University of California, Los Angeles (UCLA) Galactic Centre group

Very Large Array (VLA)

Very Large Telescope (VLT)

Very Long Base Line Array (VLBA)

XMM Newton

We list below a few papers of relevance:

MP Muno et al., Astrophysics Journal 589 (2003) 225.

F Aharonian et al., Science 307 (2005) 1938.

R Genzel et al., Nature 425 (2003) 934.

R Genzel et al., Reports of Progress in Physics 57 (1994) 417.

A Eckart et al., Astronomy and Astrophysics 450 (2006) 535.

K Baganoff et al., Astrophysics Journal 591 (2003) 901.

F Yusef-Zadeh et al., Science 287 (2000) 85.

D Rouan, Europhysicsnews 35 (2004) 141.

We also consulted the book *Black Holes and Time Warps* by Kim S. Thorne, WW Norton & Company, New York, 1994. Finally the astrophysics course of Hanoi University, P.Darriulat, *Introduction to Cosmology and Astrophysics*, Hanoi, 2004-2005, was used as a source of basic information.